



RESEARCH ARTICLE

Defect engineering in cast mono-like silicon: A review

Lihui Song¹ | Xuegong Yu²

¹College of Materials and Environmental Engineering, Hangzhou Dianzi University, No. 1, 2nd Street, Jianggan District, Hangzhou, 310018, People's Republic of China

²State Key Laboratory of Silicon Materials and Department of Materials Science and Engineering, Zhejiang University, No. 38 Zheda Road, Hangzhou, 310027, People's Republic of China

Correspondence

Lihui Song, College of Materials and Environmental Engineering, Hangzhou Dianzi University, No. 1, 2nd Street, Jianggan District, Hangzhou 310018, People's Republic of China.
Email: lhsong@hdu.edu.cn

Xuegong Yu, State Key Laboratory of Silicon Materials and Department of Materials Science and Engineering, Zhejiang University, No.38 Zheda Road, Hangzhou 310027, People's Republic of China.
Email: yuxuegong@zju.edu.cn

Funding information

National Natural Science Foundation of China, Grant/Award Numbers: 51532007 51602085 61974129 and 51532007; National Key Research and Development Project, Grant/Award Number: 2018YFB1500401

Abstract

Cast mono-like silicon is a promising material for next-generation silicon solar cells with higher efficiency and lower cost compared with currently commercialized silicon solar cells. So far, cast mono-like silicon technique still faces several problems, including multicrystallization, dislocation clusters, sub-grain boundaries, and impurity contamination, which hinder its mass-scale applications in photovoltaic industry. In this review, we will introduce these common problems in turn and discuss a multitude of the reported studies on eliminating these problems. Furthermore, light and elevated temperature-induced degradation (LeTID) was recently reported to be a severe problem of cast mono-like silicon solar cells, which can cause power loss over 10% relative. This review will introduce the behaviors and the proposed mechanisms of LeTID as well as the methods to suppress LeTID in Section 4. In the subsequent section, the efficiency potential and distribution of cast mono-like silicon solar cells are discussed. At last, a comprehensive summary will be given for this review.

KEY WORDS

cast mono-like, dislocation, light-induced degradation, solar cells, sub-grain boundary

1 | INTRODUCTION

Silicon solar cells are moving toward higher efficiency and lower cost. Cast mono-like silicon is a promising material to achieve this goal. Cast mono-like silicon was first invented by BP Solar in 2006 and then was developed by several photovoltaic companies and research institutes such as BP Solar, Solar World, and GSL. The current market share of cast mono-like silicon wafers is still less than 3%, which is much lower than the market shares of monocrystalline and multicrystalline (mc) silicon at approximately 70% and 27% in 2020, respectively. Nevertheless, because of the advantages of cast mono-like silicon, the market share of it is hoping to increase rapidly. The current global production capacity of cast mono-like silicon is roughly 10 GW, and the main players include GSL, Jinko Solar, and XYLD. According to International Technology Roadmap for Photovoltaic, the future market share for cast mono-like silicon technology will be roughly 5% in 2025. Up to now, cast mono-like silicon was typically grown by

directional solidification on multiply seeds of single-crystalline silicon, and therefore, most parts of cast mono-like silicon ingot were single crystal. Cast mono-like silicon solar cells are able to achieve higher power conversion efficiency than mc silicon solar cells, even high-performance mc (HP-mc) silicon solar cells, because of some advantages such as the availability of alkali solution to produce the inverted pyramids, and less grain boundaries (GBs). In addition, compared with Mono-Cz technology, cast mono-like silicon technology has the following advantages: (1) close efficiency with Cz silicon, (2) both are compatible with high-efficiency solar cell structure, and (3) low cost of ownership. Nevertheless, the efficiency distribution of cast mono-like silicon ingot has a long tail on low-efficiency side, which is dominantly from the top part of the ingot suffering from severe dislocation clusters, sub-GBs, and metallic impurities. These defects can significantly degrade the quality of cast mono-like silicon wafers and therefore become the focus of interest in the relevant studies.

Multicrystallization is one of the dominant challenges that cast mono-like silicon faces. Multicrystallization refers to the phenomenon that, during cast mono-like silicon growth, the mc grains nucleate randomly at the crucible walls or at the seed junctions or at the seeds' induced GBs with different grain orientations and then propagate along the growth direction. It is possible to control the area of mc grains via modulating the shape of the phase boundary between liquid and solid, the temperature distribution across the crucible, and the crystal growth rate.^{1,2} These methods can both enhance the efficiency and passed yield (wafers to cells) of the cells made on the refined wafers. Please note that the cell efficiency (PERC solar cells) and passed yield of the cells depend on the position of the wafers in the ingot.³ Typically, the wafers from the bottom part (except for "red zone") of the ingot can achieve a relatively high efficiency and passed yield (for instance, average 22.2% efficiency and 95% passed yield for PERC), whereas the wafers from the middle and top parts of the ingot can only achieve a relatively low efficiency and passed yield (for instance, <21.8% average efficiency and <90% passed yield for PERC).³ However, it should be noted that the above methods may reduce the production capability of the wafers. For example, slow crystal growth rate is able to reduce multicrystallization, but it reduces the production capability of the wafers. Furthermore, Kutsukake et al.⁴ reported the use of functional GBs, in particular $\Sigma 5$ GBs, to suppress the area of multicrystallization. This method has the advantage that it does not influence the production capability of the wafers. Nevertheless, it is found that functional GBs are not able to significantly suppress the inward extension of mc grains around the cross-points of functional GBs. Reduction of the mc grains in cast mono-like silicon ingot is an on-going task of the future research.

Dislocations and sub-GBs are other challenges of cast mono-like silicon. Most of dislocations and sub-GBs come from the seed junctions. It is reported that seed junctions between adjacent seeds, even with a small misorientation angle such as 0.02°, can produce dislocations and sub-GBs that propagate and multiply higher up along the growth direction.⁵ Functional GBs can suppress the generation and propagation of dislocations and sub-GBs. For example, Zhang et al.⁶ reported that functional $\Sigma 13$ GBs at seed junctions can prevent dislocations and sub-GBs generation and propagation along the solidification direction. However, it should be noted that $\Sigma 13$ GBs can become unstable because of small-angle deviation and be transformed to other GBs such as the $\Sigma 37$ GBs that are detrimental to the quality of cast mono-like silicon ingot. Trempa et al.⁷ also claimed that the low symmetrical GBs can avoid extensive dislocations generation at seed junctions. Furthermore, the modulation of angular deviation between the adjacent $<100>$ -oriented seeds is able to prevent dislocations generation and propagation. For instance, Hu et al.⁸ claimed that angular deviation between seeds from 10° to 45° is able to significantly control the generation of dislocations, and Wu et al.⁹ concluded a best angular deviation ranging from 10° to 30° at seed arrangements for the high-quality cast mono-like silicon ingot. In

conclusion, it is critical to control the generation or propagation of dislocations and sub-GBs for obtaining good-quality cast mono-like silicon wafers.

Metallic impurities are another challenge of cast mono-like silicon. Metallic impurities generally come from the crucible walls and diffuse into the seeds and ingot at high temperatures. So far, iron (Fe) has been identified as a harmful metallic impurity, which is responsible for the "red zone" at the bottom of cast mono-like silicon ingot. The "red zone" in cast mono-like silicon ingot (≈ 5 cm) can be as twice as the width in conventional mc silicon ingot. The researchers developed several models to explain the formation mechanisms of the "red zone." Bing et al.¹⁰ attributed the "red zone" to the back diffusion of iron impurity from the silicon melt into the seeds at the duration stage before crystal growth. However, Yu et al.¹¹ found two-peak characteristic distribution of iron at the bottom of cast mono-like silicon ingot via the variation in carrier lifetime before and after light illumination (FeB pairing and dissociation), which cannot be explained by the back-diffusion model. They explained the first iron peak to the diffusion of iron from the crucible bottom to the seeds and the second iron peak, occurring at a height of ~ 2 cm above the initial solid–liquid interface, to an iron-rich layer that formed at the initial stage of crystallization.¹¹ Please note that in the above paper, the sample has been subjected to a 1050°C annealing before characterization, and thus, all the iron precipitates should be dissolved into interstitial iron.¹² Later, Trempa et al.¹³ found that the dominant iron diffusion path from the crucible into the seeds is by gas-phase transport from furnace parts to the seeds via the furnace atmosphere rather than the direct diffusion of iron from the melt or the crucible. In addition, several approaches have been developed to suppress the "red zone" such as iron diffusion barrier layers and the reduction of duration time before crystal growth.^{10,13} Metallic impurities can also contaminate cast mono-like silicon ingot edge, which leads to nonuniformity and low stability of corresponding solar cells. To solve this problem, Hu et al.¹⁴ demonstrated GB engineering to control impurity contamination at the ingot edge. In summary, the strict control of metallic impurities into cast mono-like silicon ingot is of great importance to achieve high-quality cast mono-like silicon wafers.

Light-induced degradation (LID) has recently been found a severe problem of cast mono-like silicon wafers. The phenomenon of LID in cast mono-like silicon wafers is evident under the conditions of illumination and elevated temperatures and therefore is called "LeTID." The behaviors of LeTID in cast mono-like silicon wafers are similar to those in mc silicon wafers, although the severity is worse as reported by Sio et al.¹⁵ So far, the reported behaviors of LeTID in cast mono-like silicon wafers are briefed as follows. Please note that some studies below on LeTID are based on mc silicon solar cells, because of the limited reports about LeTID on cast mono-like silicon solar cells. First, it is found that stronger carriers' injection level, namely, higher illumination intensity or current injection and higher temperature, can accelerate the degradation of p-type mc silicon wafers.¹⁶ Second, the occurrence of degradation depends on firing peak temperature,

cooling rates of firing step, and gettering process.¹⁶ For instance, Bredemeier et al.¹⁷ claimed that severe degradation can only be observed for firing temperature at 900°C when comparing p-type mc silicon wafers fired at 900 and 650°C. Chan et al.¹⁸ further reported that substantial LeTID can only happen in p-type HP-mc silicon if the peak firing temperature exceeds 700°C. In addition, Eberle et al.¹⁹ found that slower heating and cooling rates, even with the same firing peak temperature, can reduce the extent and rate of the degradation in p-type mc silicon wafers when compared with a fast firing process. Furthermore, Zuschlag et al.²⁰ demonstrated that gettering step is able to substantially reduce the extent of the degradation in p-type mc silicon wafers. Last, the regeneration subsequent to the degradation can be accelerated by the stronger carrier injection and higher temperature.²¹ To explain the behaviors of LeTID, the mechanism of LeTID formation is extensively studied. So far, the dominant hypotheses for its formation mechanism are hydrogen- or metallic impurities-related models. For example, Vargas et al.²² found a dependence between the extent of LeTID and the amount of hydrogen released during firing in p-type mc silicon wafers, which suggested the participation of hydrogen in the formation of defect responsible for LeTID. Other researchers²¹ claimed that hydrogen either (1) acts as a detrimental force causing LeTID, for example, forming a recombination active hydrogen complex during the degradation, or (2) passivates a recombination active impurity during firing and subsequently de-passivates the impurity during the degradation. Otherwise, some researchers including Sio et al., Bredemeier et al., Eberle et al., and Jensen et al. speculated that the dissolution and reconfiguration of metallic impurities during the firing process may lead to LeTID. This hypothesis is consistent with the observation that substantial LeTID can only be formed after fast quenching, which is able to alter the structures and forms of metal precipitates.²³ Based on the mechanisms of LeTID, several methods have been proposed to suppress LeTID, including reducing the peak firing temperature,²⁴ changing the firing profile,^{18,19} rearranging the processing sequence,¹⁶ and using stronger illumination and higher temperature to accelerate the regeneration subsequent to the degradation.²⁵ These methods are effective; however, they come across the problem that they did considerable modifications to the fabrication processes of conventional silicon solar cells, which may not be feasible for the mass-scale production.²⁶ In conclusion, the behaviors of LeTID in cast mono-like silicon are similar to those in mc silicon, and a multitude of studies have reported its characteristics. The mechanism of LeTID formation is hypothesized to be related to hydrogen or metallic impurity or both of them. Nevertheless, further research is needed to clarify it. Moreover, a number of methods have been proposed to suppress LeTID, which are effective but may not be compatible with current production processes.

So far, as extensive studies have been made on cast mono-like silicon, it is the right time to give an overview on it. In this paper, we will introduce, in turn, the growth methods and conditions of cast mono-like silicon, the defects in cast mono-like silicon and the methods to suppress them, LID in cast mono-like silicon and the methods to suppress it, and finally, the cell efficiency potential and distribution of cast mono-like silicon solar cells.

2 | GROWTH METHODS AND CONDITIONS OF CAST MONO-LIKE SILICON

Cast mono-like silicon ingot is typically grown by directional solidification using single-crystalline silicon seeds. The single-crystalline silicon seeds are located at the bottom of the crucible, and generally, multiply seeds, adjacent to each other, will be used for growing cast mono-like silicon ingot. The furnace used to produce cast mono-like silicon ingot is similar to that to produce mc silicon for solar cells. The schematic diagram of the furnace is shown in Figure 1. The crystal growth is performed by controlling the temperature of the heaters in the furnace. Then, the crystal directionally grows from the melt as the melted silicon moves across the solid-liquid interface. Last, crystals with the same crystal orientation as the seeds grow epitaxially on the seeds, as shown in Figure 2. It should be noted that the seeds' crystal orientation selected is generally the <100> in consideration of the compatibility to the subsequent alkaline texturization. Furthermore, these seed tall blocks are cut from single-crystalline Czochralski (Cz) silicon ingots. The size of the seeds is typically similar to the size of solar cells, namely, $(15.6 + \alpha) \times (15.6 + \alpha) \times \text{few cm}^3$. Here, α is the kerf that occurred when cutting ingots into bricks. Multiply seeds are required to grow practical cast mono-like silicon ingots as a large-size seed, covering the whole area of the bottom of the crucible, cannot be made from Cz silicon ingots. Therefore, the boundaries between seeds are introduced into the grown ingot and become the source of sub-GBs and dislocations generation during the ingot growth. Except for the seeds, the gases flow, the crucible coating, and the silicon raw materials are similar to the casting method of mc silicon.

The processing conditions of cast mono-like silicon growth did small modifications to those in mc silicon growth. In the following paragraphs, it will discuss the temperature profile, the melt-crystal (m-c) interface, and the seed arrangements of cast mono-like silicon growth.

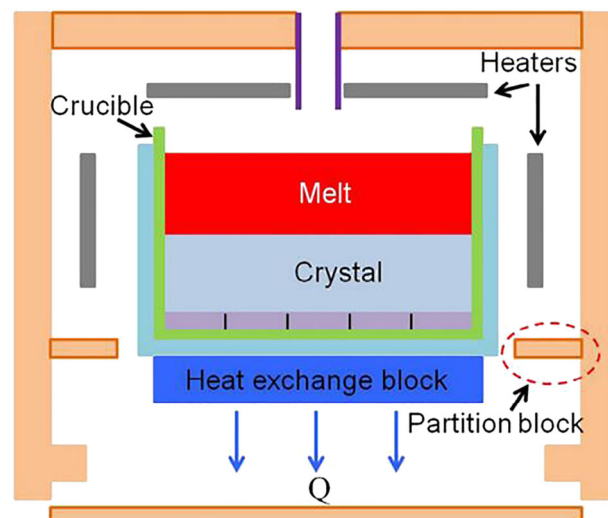


FIGURE 1 Schematic diagram of the furnace for cast mono-like silicon growth.²⁷ Reproduced from Wang et al.,²⁷ copyright 2020, WILEY Publication

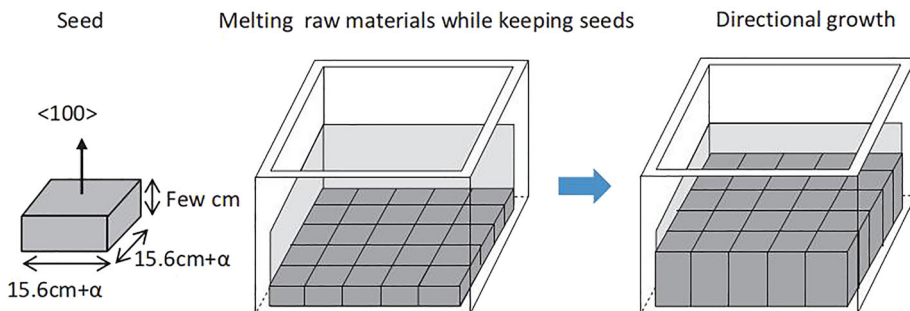


FIGURE 2 Schematic illustration of one seed and cast mono-like silicon growth.²⁸ Reproduced from Kutsukake,²⁸ copyright 2018, Springer Nature

First, we briefly introduce the temperature profile of cast mono-like silicon growth and its influences on crystal quality. The most adapted temperature profile of cast mono-like silicon growth can be influenced by argon flow rate,²⁹ the tilt of crucible,³⁰ crucible shape and size,³¹ furnace pressure,²⁹ and heater position.³² For instance, Liu et al.³³ simulated the temperature profile in a casting process using a finite-volume method in a transient way. The simulated time-dependent heater power, fraction solidified, and growth velocity during the ingots growth are shown in Figure 3. It can be seen that the crystal grew faster when the heater power decreased and then declined gradually when the heater power kept constant. The fraction of solidified silicon kept increasing until unity. The paper also simulated the temperature distribution and melt flow pattern in the solidified ingot when half of the ingot had been grown, as shown in Figure 4. In Figure 4, it can be seen that two weak vortices formed in the melt and the flow velocity of the melt is estimated to be the order of several mm/s, which is nearly one order of magnitude smaller than that in Cz silicon growth. It can also be found that the crystal-melt interface is concave to the solidified part, and the simulations revealed that the temperature gradient in the solid was approximately 10 K/cm that was roughly one third or one fourth of the value in Cz silicon growth. Li et al.²⁹ investigated the effects of argon flow rate and furnace pressure on the temperature profile in a directional solidification

furnace. It was found that the enhanced argon flow rate can increase the ratio of convective heat transfer to radiative heat transfer and the gas shear stress at the melt-free surface, resulting in an alteration in the temperature profile. Furthermore, the reduction in furnace pressure was found to enhance the effect of argon flow on the temperature profile. These observations implied that the most adapted temperature profile in a directional solidification process could be controlled by the argon flow rate and the furnace pressure. Moreover, Miyazawa et al.³⁰ reported that the tilt of crucible can modify the temperature profile three dimensionally in the furnace. The temperature profile plays an important role on the crystal quality. It is known that nonuniform thermal deformation can lead to thermal stresses, resulting in dislocation generation. To overcome this problem, Yang et al.³⁴ reported that a small temperature gradient was able to reduce the thermal stresses in the grown ingot as well as provided a suitable m-c interface shape for crystal growth. Chen et al.³⁵ reported that thermal stresses can be reduced via the modification of the thermal field. In conclusion, the temperature profile should be carefully controlled to improve the quality of the grown ingot.

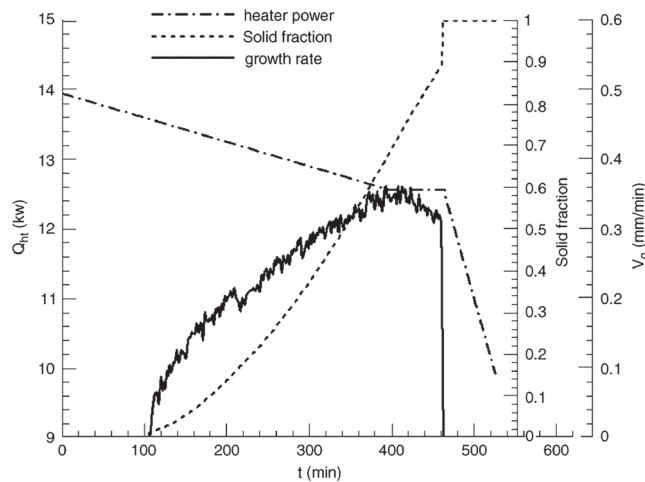


FIGURE 3 Heater power, fraction solidified and growth rate as a function of time during the crystal growth.³³ Reproduced from Liu et al.,³³ copyright 2006, Elsevier B.V

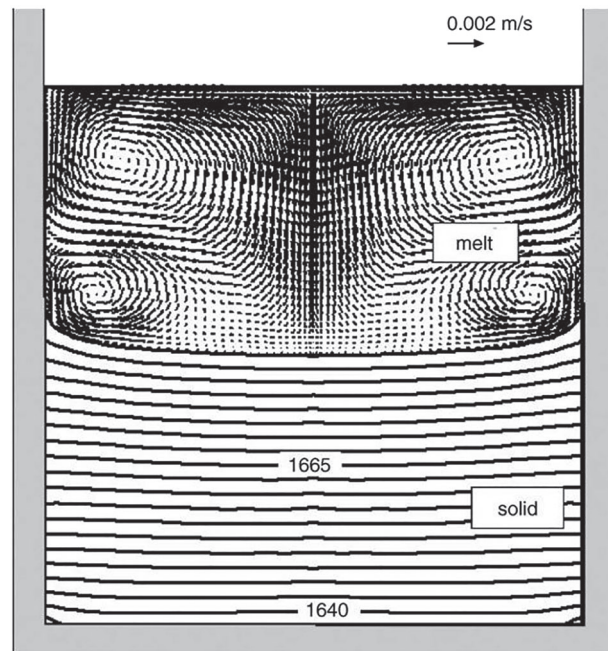


FIGURE 4 Temperature distribution and melt convection during the ingot growth. The unit for temperature is Kelvin.³³ Reproduced from Liu et al.,³³ copyright 2006, Elsevier B.V

Second, we briefly introduce the influences of the processing conditions on the m-c interface and the consequent influences on crystal quality. It was reported that the crucible shape and dimensions,³¹ the argon flow rate,³⁶ and crystal growth rate³⁷ can influence the shape of the m-c interface. In detail, Miyazawa et al.³¹ found that square crucible can induce a maximum deformation of the m-c interface near the corner of the crucible, as shown in Figure 5. Li et al.³⁶ claimed that the argon flow can modify the m-c interface via altering the pattern and intensity of the melt convection at the middle stage of the solidification process. Furthermore, at the final stage of solidification, an increase in argon flow rate can make the m-c interface more convex to the melt, which is because of the cooling effects of the argon gas flow. Li et al.³⁷ also reported that high crystal growth rate, associated with a fast cooling process, made the m-c interface convex to the crystal, whereas medium and slow crystal growth rates produced a relatively flat m-c interface. The m-c interface plays a significant role on crystal quality. It was reported that the m-c interface shape has a dramatic effect on the magnitude of thermal stress, which is responsible for dislocation generation. For instance, Hu et al.³⁸ reported the modifications of the power ratio and insulation gap in order to make the m-c interface convex to the melt consistently during the crystal growth, resulting in a 41% reduction in thermal stress and an 80% reduction in dislocation generation. Teng et al.³⁹ found that a slightly higher convexity of the m-c interface in the central region was beneficial for reducing the strength of the melt flow convection so as to obtain a more uniform carbon distribution in the melt. In one word, it is crucial to control the m-c interface in order to obtain a good quality silicon ingot.

Last, a comparison between a relatively large-size seed and multiply small-size seeds is made in terms of their impacts on crystal

quality. Normally, multiply small-size Cz silicon seeds are used for cast mono-like silicon ingot growth in order to cover the whole area of the bottom of the crucible. However, the joints between seeds inevitably introduce the boundaries into the grown crystal, which become the source of dislocations and sub-GBs generation during the solidification.⁴⁰ These dislocations and sub-GBs will propagate and multiply higher up along the growth direction and thus form a multitude of dislocation clusters in the upper part of ingot. The detailed mechanisms of dislocations and sub-GBs generation will be discussed in Section 3. A single and relatively large seed instead of multiply small seeds placed at the center of the bottom of the crucible can avoid the introduction of the boundaries at seed joints. Nevertheless, because of the technical limitation of the size of Cz silicon seed, a single seed is impossible to cover the whole bottom of a large crucible, and therefore, some random orientation crystal may nucleate at the bottom of the crucible. Numerical simulations² revealed that the crystal growth from one single seed was like a mushroom-type interface growth. In addition, Miyamura et al.⁴¹ demonstrated in an experiment that cast mono-like silicon ingot was possible to be grown from one single seed via controlling the thermal flux in the furnace. However, the dendritic growth occurred at the top surface. In summary, multiply small-size seeds are favored for cast mono-like silicon production in industry; however, special attention should be paid to mitigating the dislocations generation from seed joints.

In this section, the processing conditions and sequences of cast mono-like silicon growth are reviewed. In particular, the thermal profile, m-c interface, and seed arrangements are discussed in detail in terms of the factors to modify them and their influences on crystal quality. In general, it is concluded that a uniform temperature profile and a slightly convex m-c interface to the melt and multiply seeds are optimal options for cast mono-like silicon growth.

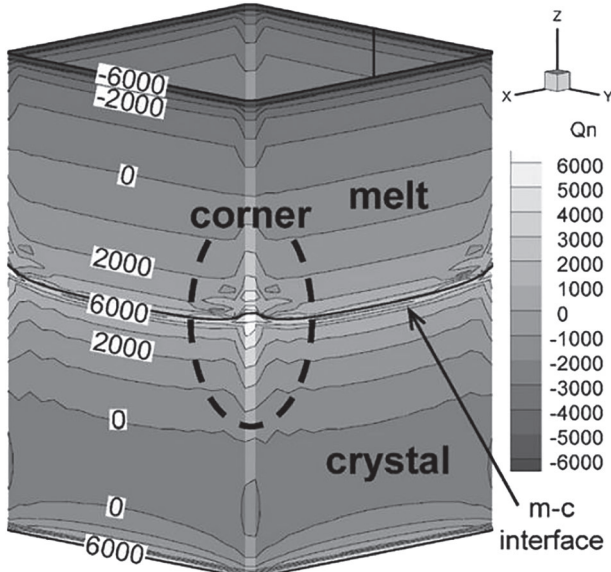


FIGURE 5 Melt-crystal (m-c) interface during the crystal growth.³¹ The circle marks the m-c interface shape at the corner of the square crucible. Reproduced from Miyazawa et al.,³¹ copyright 2008, Elsevier B.V.

3 | DEFECTS IN CAST MONO-LIKE SILICON AND METHODS TO SUPPRESS THEM

As mentioned above, it is inevitable to introduce defects into the grown ingot because of the practical growth conditions. Therefore, it is crucial to understand the mechanisms of the defects generation and find methods to suppress them. So far, a multitude of studies have reported various kinds of defects in cast mono-like silicon ingot, including four categories, namely, multicrystallization, dislocations, sub-GBs, and impurity contamination. In this section, the origins of these defects and the developed methods to suppress them are discussed and analyzed.

3.1 | Multicrystallization

Multicrystallization is a common problem in cast mono-like silicon ingot. During the cast mono-like silicon growth, various grains with a different crystallographic orientation nucleate at random sites on the

inner side walls of the crucible and then extend directionally inside the ingot. As a consequence, the cast mono-like silicon wafers become partially mc along the crucible walls.⁴² Multicrystallization leads to a significant reduction in power conversion efficiency. For instance, the solar cells made from cast mono-like silicon wafers lose performance with an increase in the area of mc region and do not show a gain in power conversion efficiency when the mc region exceeds 30% of the total area.⁴

Multicrystallization can be suppressed by controlling the growth conditions such as the temperature distribution, m-c interface shape, and crystal growth rate. In detail, Gao et al.² reported that the area of mc grains is determined by a ratio of thermal flux along the crucible wall to thermal flux along the seed, and therefore, multicrystallization can be dramatically reduced either by reducing the thermal flux along the crucible wall or by increasing the thermal flux along the seed. Liu et al.⁴³ demonstrated that a down-up moving partition block was able to keep the m-c interface flat or slightly convex to the melt consistently during the solidification process, resulting in a markedly reduced mc region. Furthermore, Gao et al.² also reported that an optimized furnace structure was able to make the m-c interface march toward the crucible wall so as to minimize the area of mc region. As reported, controlling the growth conditions is an effective way to suppress multicrystallization; however, it may reduce the production capability of the wafers.

Multicrystallization can also be suppressed by functional GBs. Kutsukake et al.⁴ reported the use of functional $\Sigma 5$ GBs to successfully limit the mc region to a small area close to the crucible wall, as shown in Figure 6. In detail, $\{111\} \Sigma 3$ GBs frequently form at the crucible side walls accompanied by nucleation of mc grains. In the case of the cast mono-like silicon ingot with $\Sigma 5$ functional GBs, the $\{111\} \Sigma 3$ GBs interacting with the $\Sigma 5$ functional GBs to be converted into $\{310\} \Sigma 15$ GBs, as shown in Figure 7. The $\{310\} \Sigma 15$ GBs have a stable configuration in the [001] crystal orientation and expand straight in the growth direction, which is able to prevent the extension of mc grains. However, the results also revealed that the inward extension of mc grains still existed around the cross points of functional GBs. In conclusion, functional GBs are able to confine mc region to the periphery of the ingot, which is not used for solar cell wafers because of high impurity contamination. Furthermore, the method of functional GBs is not necessary to modify the crystal growth conditions, and therefore, it can still maintain high production capability of the wafers.

In summary, multicrystallization is a common problem to cast mono-like silicon. It can be suppressed by controlling the crystal growth conditions; however, this may alter the optimal growth conditions. In addition, functional GBs can suppress the extension of mc grains, and it has the advantage that it can be compatible with a range of growth conditions.

3.2 | Dislocations

Dislocations are one of the dominant defects in cast mono-like silicon, which are detrimental to the performance of the corresponding solar

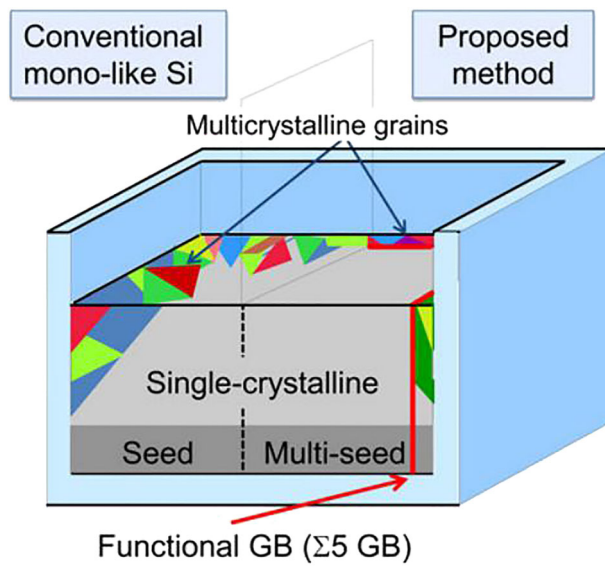


FIGURE 6 Schematic illustration of conventional cast mono-like silicon method (left) and the refined method by functional grain boundaries (GBs) (right).⁴ Reproduced from Kutsukake et al.,⁴ copyright 2014, IEEE

cells. In cast mono-like silicon method, dislocations typically generate from the GBs formed at the seed joints and then propagate and multiply higher up along the growth direction. To further improve the quality of cast mono-like silicon, it is crucial to understand the mechanisms of dislocation generation and propagation and find the solutions to suppress them.

The mechanisms of cellular dislocation generation in cast mono-like silicon ingot were extensively studied, and these studies dominantly focus on two types of investigations: the influence of the GB microstructure and the influence of the stress distribution.

Dislocations generated from small angle and CSL GBs are sensitive to the microstructure of the GBs such as the misorientation angle

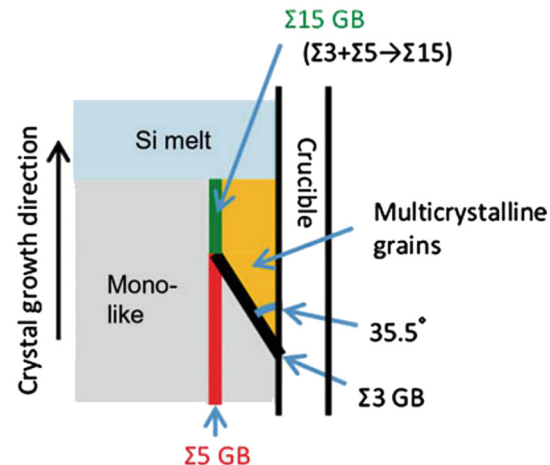


FIGURE 7 Schematic illustration of the method to suppress multicrystallization.²⁸ Reproduced from Kutsukake,²⁸ copyright 2018, Springer Nature

and its components. Wu et al.⁹ experimentally demonstrated that a $\sim 0^\circ$ -tilt GBs generated cellular dislocations more easily than large-angle tilt GBs during the crystal growth, which conformed to the hypothesis that dislocation generation from a small-angle GB is more sensitive to the microstructure compared with that from a large-angle random GB. In addition, Ekstrøm et al.⁴⁴ systematically investigated the effects of the misorientation angle of a small-angle GB on the cellular dislocation generation. They found that, in the junctions containing no or small gaps, the amount of dislocations generated dominantly depended on the misorientation angle between the adjacent seeds. The gaps between adjacent seeds, as another important parameter that determines the microstructure of GBs, can also influence the cellular dislocation generation at seed joints. For instance, Trempa et al.⁴⁵ reported that cellular dislocations were generated at the seed edges and in the gap center because of the thermal shock of the silicon melt and the lattice mismatch of two growth front, respectively. Note that even small deviation angles of $<1^\circ$ of the adjacent seeds are able to induce the lattice mismatch of two growth front, resulting in dislocation and small-angle GBs generation. The cellular dislocations generated in the seed gaps are shown in Figure 8. They also concluded that small seed gaps with highly aligned seed pieces were beneficial to growing high-quality cast mono-like silicon ingot.

On the other hand, cellular dislocations generated from a random GB are sensitive to the stress around the GBs rather than the microstructure. In detail, Takahashi et al.⁴⁶ reported that the amount of dislocations generated from a random GB demonstrated a positive correlation with the magnitude of the numerically calculated shear stress. Usami et al.⁴⁷ also claimed that dislocation density was in good correlation with the shear stress around the random GBs.

Except for the mechanisms of dislocation generation, a multitude of studies have investigated the methods to suppress dislocation generation and propagation. So far, special GBs, functional defects, different crystal orientations, and seed partitions have been reported to mitigate dislocation generation and propagation successfully. For the

method of special GBs, Hu et al.⁸ reported that special GBs between the adjacent seeds with twisted angular deviations of 10° – 45° were able to remarkably suppress dislocation generation from seed joints, resulting in an average power conversion efficiency of the aluminum (Al) back surface field (BSF) solar cells at 18.1% with an absolute 0.6% efficiency enhancement. Although special GBs were able to mitigate dislocation generation significantly, it may increase the complexity of seed preparation and induce the problem of color mismatch.⁴⁸ For the method of functional defects, Takahashi et al.⁴⁹ reported the use of functional defects (SMART) to block the propagation of dislocations into the central region of the ingot. Figure 9 shows a schematic illustration of SMART technique. The SMART technique used one type of functional GB to generate dislocations and another type of functional GB to block dislocation propagation. The intentionally introduced dislocations could reduce the stress during the crystal growth, which was able to mitigate the dislocation generation in the central region of the ingot. As a result, the dislocations were confined in a thin region of the ingot that was normally disposed because of impurity contamination. For the method of seed partitions, Lan et al.⁴⁸ used thin silicon plate seeds with a 30° or -30° tilt angle from both sides of the seed crystals to act as seed partitions. As a consequence, two parallel GBs were formed in seed joints and were able to effectively suppress dislocation generation from seed joints. Two advantages of this method were emphasized: (1) It was easy for seed preparation as the main seeds had the same three-dimensional crystal orientation; (2) it could avoid the problem of color mismatch.

It is worth mentioning that hydrogen, introduced during the cell fabrication processes, is able to effectively passivate dislocations in the cast mono-like silicon wafers, so as to minimize the detrimental effects of dislocations on the completed solar cells. In the early, Divigalpitiya et al.⁵⁰ found that dislocations in crystalline silicon can be passivated by hydrogen plasma, resulting in a reduction in dark saturation current and an increase in open-circuit voltage of the cell. Later, Martinuzzi et al.⁵¹ reported that hydrogen released from $\text{SiN}_x\text{:H}$

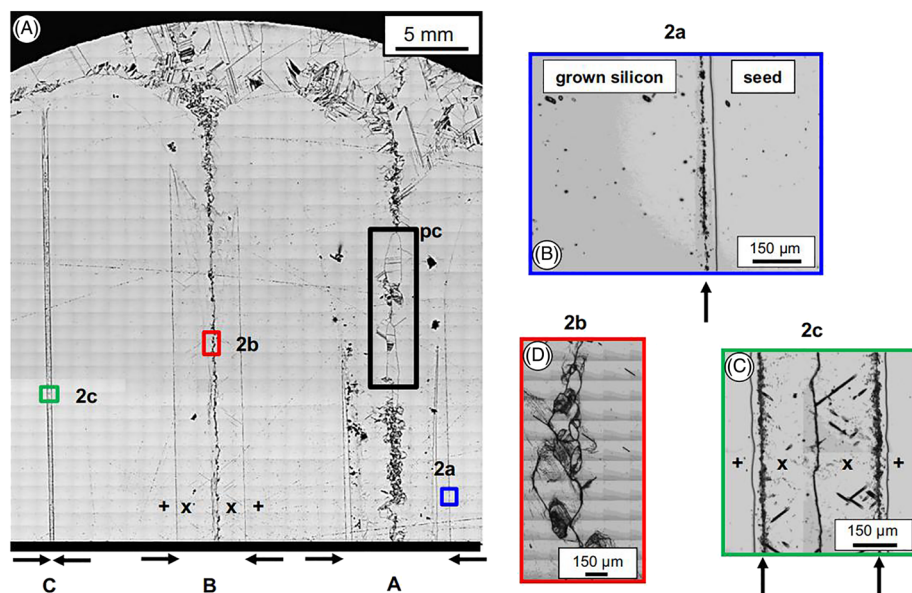


FIGURE 8 Optical micrograph of dislocations generated in the seed gaps: A, 10-mm gap; B, 5-mm gap; and C, <1 -mm gap. The black arrows indicate the position of seed edges. The rectangular areas 2a, 2b, and 2c are magnified on the right hand side (b-d).⁴⁵ Reproduced from Trempa et al.,⁴⁵ copyright 2014, Elsevier B.V.

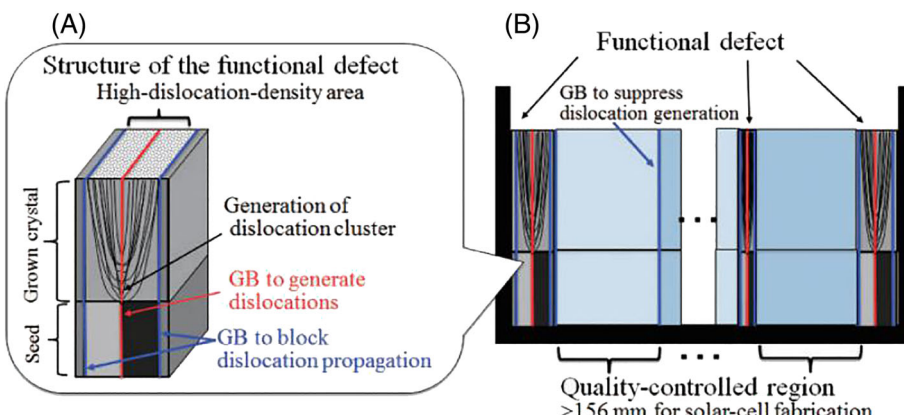


FIGURE 9 Schematic illustration of the SMART method. (A) Structure of the functional defect and (B) the grown ingot in a crucible.⁴⁹ Reproduced from Takahashi et al.,⁴⁹ copyright 2015, The Japan Society of Applied Physics

layer could passivate dislocation clusters and transformed the deep levels associated with the dislocation clusters into the shallow levels. In the recent decade, Song et al.⁵² demonstrated that postfiring hydrogenation step, via an illuminated annealing process at 350°C and 9.6×10^{18} photons/cm²/s illumination intensity for 4 min, could further enhance the passivation of dislocation clusters in the cast mono-like silicon solar cells (as illustrated in Figure 10). The above result indicates that dislocation passivation by hydrogen needs a relatively long treatment time (in the order of several minutes) at low temperature compared with fast-firing process.

In summary, dislocations are one of the most harmful defects to cast mono-like silicon. The mechanisms of dislocation generation are either sensitive to the microstructure of the GBs or sensitive to the stresses around the GBs. The methods to mitigate dislocation generation or propagation are extensively studied and incorporate special GBs, functional defects, different crystal orientations, and seed partitions up to date. Dislocations can be passivated by hydrogen, generally released from the SiN_x:H layer, and the deep levels associated with dislocation clusters would be transformed into the shallow levels after hydrogen passivation. Recent study indicated that effective passivation of dislocation clusters in cast mono-like silicon by hydrogen needed a relatively long treatment time.

3.3 | Sub-GBs

Sub-GB is another dominant defect in cast mono-like silicon wafers. Indentation damage on seed surface and seed junctions can be the sources of sub-GB generation. Once generated, sub-GBs multiply and propagate higher up along the crystal growth direction. Furthermore, sub-GBs are able to cause highly and inhomogeneously distorted regions along them, which attract impurity precipitating in and near these regions. The presence of impurity precipitation in and near the sub-GBs contributes to the dislocation generation and then dislocations propagate away from the sub-GBs during the crystal growth. In this section, we will briefly introduce the mechanisms of sub-GBs generation and the influences of sub-GBs on the crystal quality.

The generation of sub-GBs can be induced by either indentation damage on seed surface or seed joints. Oliveira et al.⁴⁰ reported that feedstock indentation on seeds can cause sub-GBs on the contact points, as shown in Figure 11. Tsoutsouva et al.^{5,53} pointed out that the relative misorientation as small as 0.02° between two seeds was able to induce highly and inhomogeneously distorted sub-GBs, as shown in Figure 12.

The influences of sub-GBs on the quality of cast mono-like silicon ingot are significant. Sub-GBs can be the origin of dislocation

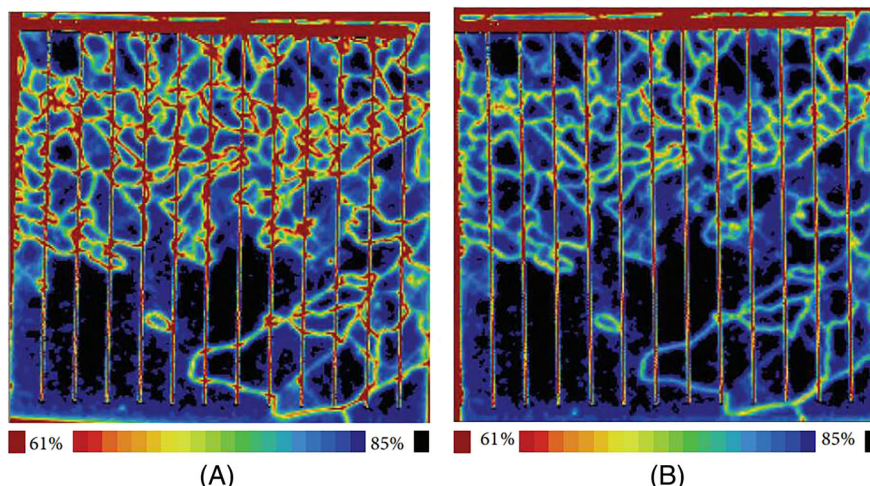


FIGURE 10 LBIC scan map of the p-type cast mono-like silicon solar cell (A) before postfiring hydrogenation step and (B) after postfiring hydrogenation step. Reproduced from Song et al.,⁵² copyright 2015, Hindawi Publishing Corporation

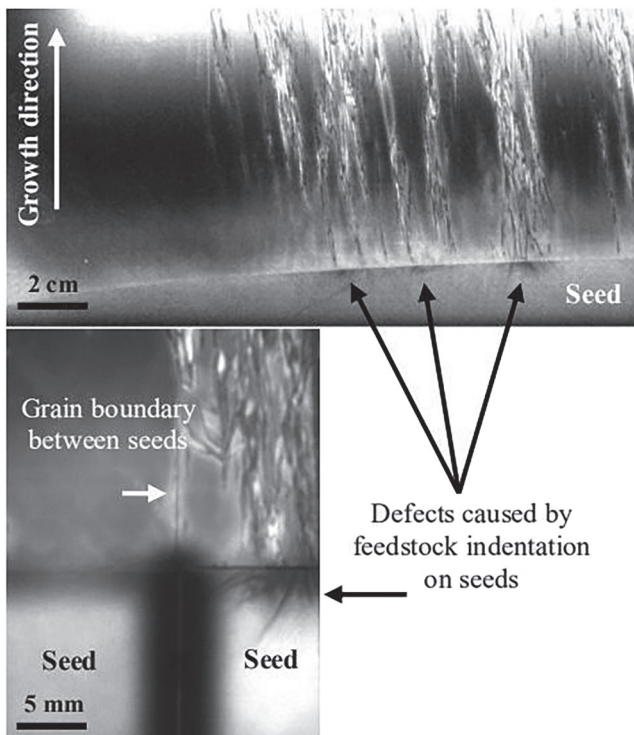


FIGURE 11 Sub-grain boundaries generated by feedstock indentation on seeds.⁴⁰ Reproduced from de Oliveira,⁴⁰ copyright 2014, 29th European Photovoltaic Solar Energy Conference and Exhibition

generation and the sink for impurity precipitation. Ryningen et al.⁵⁴ reported that dislocations can generate from sub-GBs and subsequently propagate higher up along the crystal growth direction. Tsoutsouva et al.⁵³ confirmed that sub-GBs are the major sources for the development of dislocation cascades and clusters and also reported that the impurities such as N, O, and C preferentially precipitated along sub-GBs, as shown in Figure 13. Moralejo et al.⁵⁵ found that impurities were inhomogeneously distributed at the sub-GBs and the impurity decorated sub-GBs showed stronger recombination activities compared with “clean” sub-GBs.

The methods to suppress sub-GBs generation include the careful alignment of seeds to minimize the misorientation angle as low as possible and a before-cast preparation of the feedstock to avoid the sharp points.⁴⁰ For instance, Zhang et al.⁶ reported that the artificially designed $\Sigma 13$ GBs between two adjacent $<100>$ -oriented seeds can remarkably suppress the generation of sub-GBs, as shown in Figure 14. In addition, Zhang et al.⁵⁶ recently demonstrated that $<110>$ -oriented seeds were able to mitigate the cascade shape of sub-GBs in the ingot and hence resulted in a better internal quantum efficiency (IQE) of the wafers. Figure 15 reveals the carrier lifetime mappings on the cross sections of $<100>$ - and $<110>$ -oriented cast mono-like silicon ingots, respectively.

In conclusion, sub-GBs can be generated from either indentation damage on seed surface or seed joints. It is worth noting that a relative misorientation angle between two seeds as small as 0.02° can

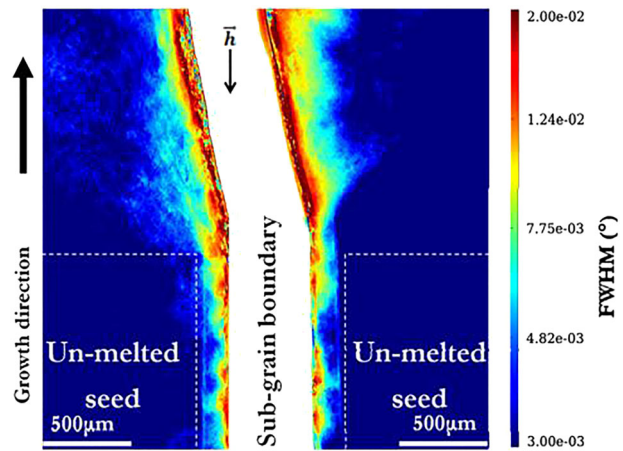


FIGURE 12 X-ray RCI FWHM map of the Si 004 reflection in the area between two seeds that leads to the formation of the sub-grain boundary.⁵³ Reproduced from Tsoutsouva et al.,⁵³ copyright 2014, Elsevier B.V

induce sub-GBs at seed joints. Furthermore, the formed sub-GBs are the sources of dislocation generation and impurity precipitation. Therefore, it is crucial to suppress sub-GBs generation to obtain high-quality cast mono-like silicon ingot.

3.4 | Impurities

Crucible and its coating typically contain large amount of impurities that can contaminate cast mono-like silicon ingot during crystal growth. Impurities such as iron and oxygen diffuse into the side and the bottom of the ingot from crucible, and thus, it results in low carrier lifetime zones. Among these low carrier lifetime zones, “red zone” at the bottom of the cast mono-like silicon ingot is the severest problem. “Red zone” (≈ 5 cm) in cast mono-like silicon ingot can be twice as wide as that found in conventional cast mc silicon, which significantly reduce the yield of cast mono-like silicon ingot. Red zone can reduce the carrier lifetime of p-type cast mono-like silicon wafers by more than two orders of magnitude and the material yield (the number of wafers qualified for producing solar cells/the total number of wafers from the red zone of the ingot) by one order of magnitude.⁵⁷ As reported, “red zone” is mainly attributed to the iron contamination; however, there are various hypotheses for the detailed mechanisms. We will discuss the various hypotheses for the mechanisms associated with the formation of “red zone” in the next paragraph. In addition, impurities were also able to segregate at the sub-GBs and therefore enhance their recombination activities. We will discuss more about impurity segregation at the sub-GBs next to the discussion of “red zone.” At last, impurity contamination at the ingot edge is discussed.

“Red zone” typically refers to a low carrier lifetime zone at the bottom of the ingot. For cast mono-like silicon ingot, the width of “red zone” can be twice as wide as that found in conventional cast mc silicon. The widely accepted explanation for the formation of “red zone”

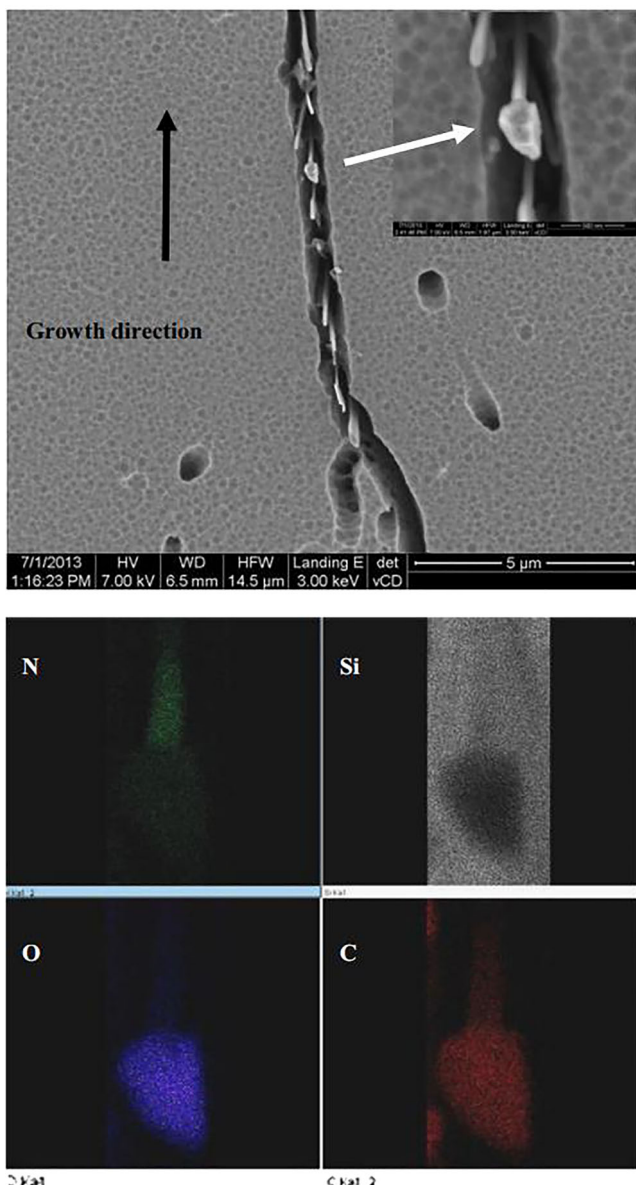


FIGURE 13 SEM image and EDX maps of $\text{Si}_x\text{C}_y\text{O}_z$ and Si_3N_4 precipitates in the sub-grain boundary.⁵³ Reproduced from Tsoutsouva et al.,⁵³ copyright 2014, Elsevier B.V.

is attributed to the high concentration of iron impurities diffusing from the quartz crucible. Nevertheless, there are several hypotheses for the reasons associated with the wider width of “red zone” in cast mono-like silicon ingot. Gao et al.¹⁰ reported a low-high-low nonmonotonic distribution of iron impurities at the bottom of the ingot, as shown in Figure 16. They attributed it to the back diffusion of iron impurity from silicon melt into the seed at the duration stage before crystal growth. However, Yu et al.¹¹ found that the second iron peak was not located at the solid/melt interface and thus argued that the back diffusion model cannot explain the second iron peak. They claimed that the first iron peak was due to iron diffusion from the crucible and the second iron peak was due to the formation of an iron-rich layer at the initial stage of crystallization, as shown in Figure 17.

Furthermore, Trempa et al.¹³ investigated the iron diffusion path from the crucible into the seed and found that gas-phase transport from furnace parts to the seeds via furnace atmosphere was an important iron contamination path.

The methods to reduce the width of “red zone” in cast mono-like silicon ingot can be several. As the formation of “red zone” is associated with the iron contamination from the crucible, it is possible to reduce the width of “red zone” by using the crucible with low iron content. In addition, Gao et al.⁵⁸ suggested that the back diffusion of iron impurities from the melt into the seed was the main reason for the formation of “red zone,” and therefore, it is essential to reduce the duration time before crystal growth to reduce the width of “red zone.” Furthermore, Trempa et al.¹³ reported the use of iron diffusion barriers to reduce the width of “red zone” in cast mono-like silicon ingot.

Except for the problem of “red zone,” impurities from the crucible are also able to segregate at the crystallographic defects to enhance their recombination activities. Ohno et al.⁵⁹ reported that nickel (Ni), copper (Cu), and oxygen atoms preferentially segregated at the sub-GBs with arrays of dislocations. Furthermore, it was found that the concentration of Ni and Cu were in a trade-off correlation with that of oxygen in the sub-GBs, whereas the total numbers were almost a constant independent of the characters of the sub-GBs. Therefore, it can be concluded that the segregation of oxygen atoms at the sub-GBs would be better for solar cells, as it can reduce the number of the metallic impurities at the sub-GBs. Hayama et al.⁶⁰ also found that interstitial iron impurities would be precipitated at the area of high dislocation density upon annealing at 600°C. In addition, Tsoutsouva et al.⁵³ reported that impurities such as C, O, and N tended to precipitate in and near the sub-GBs, which contribute to the generation of dislocations. So far, it was reported that the use of crucible with low impurity content and artificially designed high dislocation regions at the periphery of the ingot could be feasible for reducing impurity contamination in the central region of the ingot.^{53,60}

Impurity at the ingot edge can also be a severe problem, which leads to nonuniformity and low stability of corresponding solar cells. For instance, iron in-diffusion from crucible walls can result in a narrow low carrier lifetime zone at the ingot edges with a width of about 2 cm. This narrow low lifetime zone may develop into hot spots during the long-time operation and finally cause break-down in p-n junction.^{61,62} Some methods can be used to suppress impurity contamination at the ingot edges. Crucible with low impurity content and SiN_x coating on crucible walls are apparent options; however, they unavoidably increase the fabrication cost of wafers. In addition, Hu et al.¹⁴ demonstrated GB engineering to control impurity contamination at the ingot edge. They used the silicon powder coating layer at crucible walls to control the nucleation of grains at the ingot edges, which induces parallel GBs along the crucible walls. The resultant GBs can getter iron impurity and meanwhile become barriers for iron in-diffusion. As a consequence, the low lifetime zone at the ingot edges is significantly reduced, as shown in Figure 18.

Light elements such as C, N, and O also play an important role on the electrical properties of the cast mono-like silicon wafers. Oxygen typically exists in the form of interstitial oxygen in the as-grown cast

FIGURE 14 PL images of the wafers from the bottom (a1,b1), the middle (a2,b2), and the top (a3,b3) of the blocks from ingot A (a) with small-angle grain boundaries (GBs) and ingot B (b) with special GBs. The red rectangle indicates that the special GBs suppress the propagation of sub-GBs.⁸ Reproduced from Hu et al.,⁸ copyright 2015, Elsevier B.V.

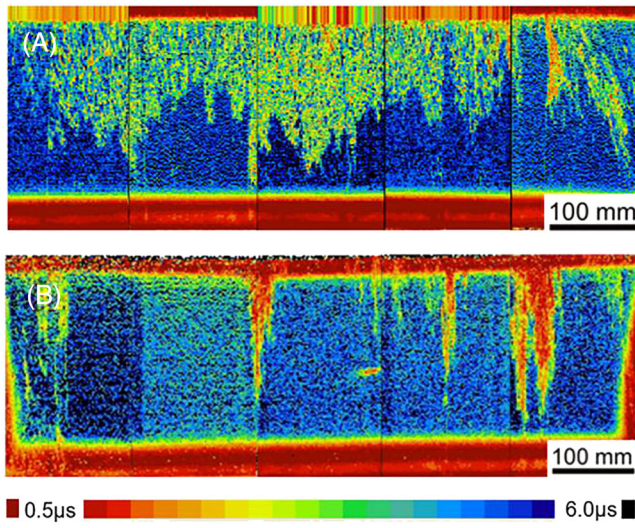
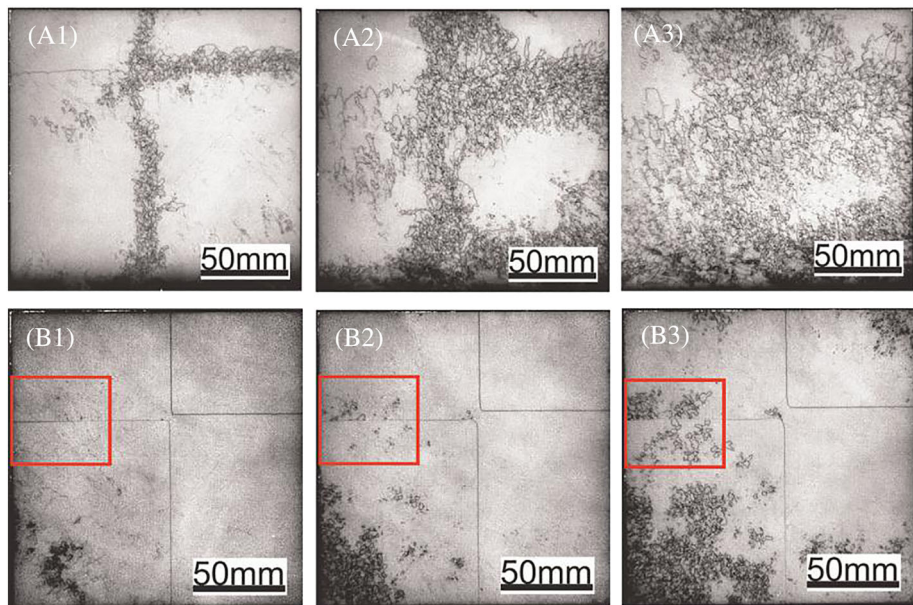


FIGURE 15 Carrier lifetime mappings on the cross sections of (A) <100>-oriented cast mono-like silicon ingot and (B) <110>-oriented cast mono-like silicon ingot.⁵⁶ Reproduced from Zhang et al.,⁵⁶ copyright 2019, Elsevier B.V.

mono-like silicon wafers, and its concentration is in the order of $\sim 1 \times 10^{17} \text{ cm}^{-3}$, which is lower than the typical interstitial oxygen concentration (roughly 2×10^{17} to $1.0 \times 10^{18} \text{ cm}^{-3}$) in Cz silicon.⁶³ Interstitial oxygen typically can form thermal donors in the temperature range of 300–500°C in Cz silicon, and these thermal donors will be dissociated when the temperature is above 500°C.⁶³ However, the high C density in cast mono-like silicon will retard the formation of thermal donors in cast mono-like silicon, and therefore, only few thermal donors are present in cast mono-like silicon.⁶⁴ Precipitation of oxygen typically occurs during crystal growth and subsequent thermal processes in the Cz cell fabrication. Generally, oxygen precipitates form nucleus at the temperature of approximately 800°C and grow up

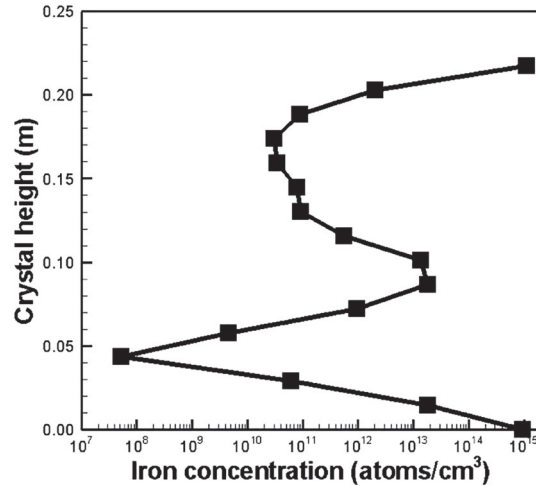


FIGURE 16 Iron concentration profile at the bottom of the ingot along the crystal growth direction.¹⁰ Reproduced from Bing et al.,¹⁰ copyright 2011, American Chemical Society

at the temperature of $\sim 1000^\circ\text{C}$. As far as the authors know, no grown in oxygen precipitates are observed in cast mono-like silicon⁶⁵; however, oxygen precipitation can occur during the subsequent high-temperature process. It is worth noting that high C density in cast mono-like silicon can enhance the oxygen precipitation.⁶⁵ The reasons are in two ways. Below a critical temperature in the range of 800–850°C, the C-O complex can act as heterogeneous nucleation centers for oxygen precipitation,⁶⁵ whereas above the critical temperature, C plays a catalytic role in oxygen precipitation.⁶⁵ Oxygen precipitates are severe recombination centers, and therefore, they should be carefully controlled during the cell fabrication process. Carbon generally occupies the substitutional position, and the concentration of the substitutional carbon is approximately $3.0 \times 10^{17} \text{ cm}^{-3}$ in the cast mono-like silicon compared with roughly $5.0 \times 10^{16} \text{ cm}^{-3}$ in Cz

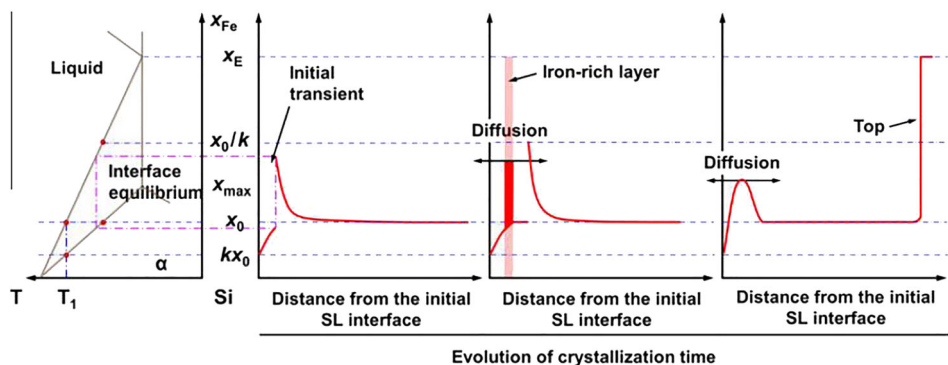


FIGURE 17 Schematic diagram of the formation mechanism of the second iron peak during crystal growth.¹¹ Reproduced from Yu et al.,¹¹ copyright 2013, Elsevier B.V.

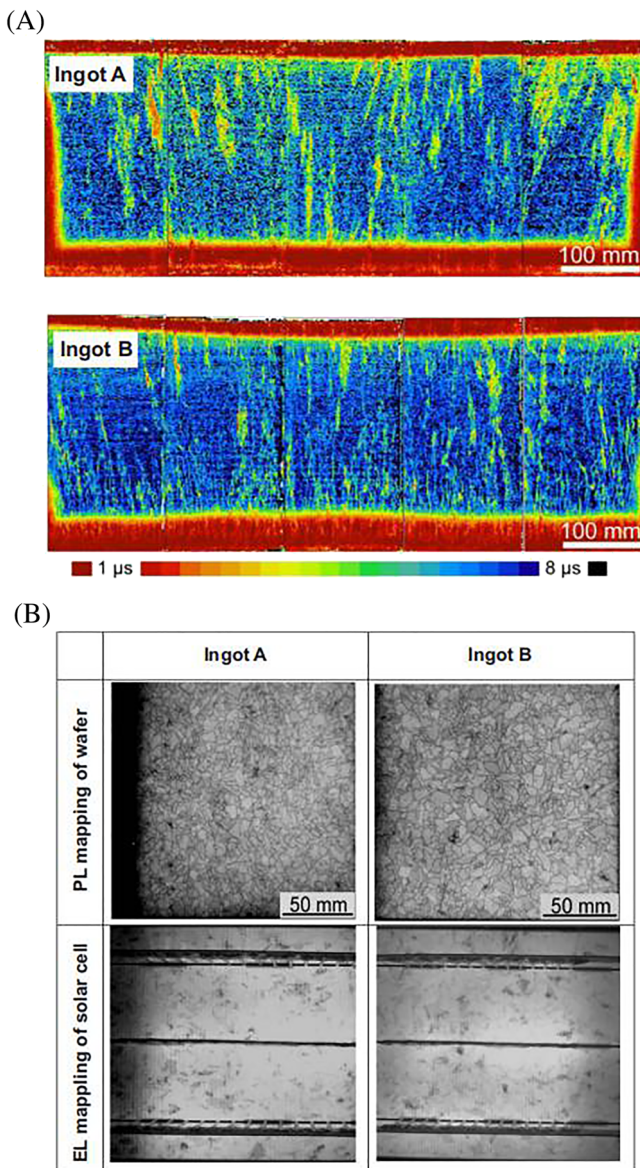


FIGURE 18 (A) Carrier lifetime mappings of the cross sections and (B) PL/EL mappings of the side brick wafers and corresponding solar cells from ingots A and B. Here, ingot A is the standard silicon ingot, and ingot B is the ingot applied with grain boundary engineering.¹⁴ Reproduced from Hu et al.,¹⁴ copyright 2017, Elsevier B.V.

silicon.⁶⁶ The dissolved carbon, existing as substitutional atoms, is electrically inactive, but it can strongly influence the density and electrical activity of dislocations in cast mono-like silicon.⁶⁷ When the concentration of carbon exceeds its solubility in silicon during the crystal growth, it will precipitate in the form of silicon carbide (SiC), which can cause severe ohmic shunting across the p-n junction. The precipitates of SiC typically have two forms—particles and filaments in cast mono-like silicon.⁶⁸ The SiC filaments are <5 μm in diameter but up to 3 mm in length.^{68,69} The SiC filaments mostly grow in GBs and in the direction of crystallization direction.⁶⁹ The SiC filaments are typically doped with N impurity at the concentration of $1.3\text{--}2.8 \times 10^{21}$ atoms/cm³ and hence are n-type.^{68,69} Because of the high N doping in the SiC filaments, the SiC filaments can be a low-resistant shunting path for cast mono-like silicon solar cells. The SiC particles are 1–600 μm in diameter. The SiC particles are also highly doped with N impurity at the concentration of $\sim 10^{21}$ atoms/cm³; however, because of the small length of the SiC particles, they are less likely to cause shunting problem.⁶⁸ In addition, the SiC particles mostly grow within grain volume and around the Si₃N₄ rod.⁶⁸ More information about the SiC precipitates in cast mono-like silicon can be found elsewhere.^{68–70} The N concentration in cast mono-like silicon is in the range of $4\text{--}6 \times 10^{15}$ cm⁻³.⁷¹ In cast mono-like silicon, nitrogen (N) atoms exist in the forms of monomer, dimer, complex, and precipitates. Nitrogen monomer, generally in the form of substitutional nitrogen atom, only accounts for 1% of total N atoms in silicon and does not influence the electrical properties of silicon much.⁷² N dimer and N-O complex are the main form of N in silicon under room temperature. N dimer is inactive in silicon, whereas N-O complex serves as thermal donors in silicon, which can vary the resistivity of n- and p-type silicon wafers.⁷² Moreover, N dimer and N-O complex are found to increase the mechanical strength of the silicon wafers.⁷² When the N concentration exceeds its solubility, the Si₃N₄ precipitates form in silicon. The Si₃N₄ precipitates in cast mono-like silicon are in three forms: rods, fibers, and nets. The Si₃N₄ rods are <30 μm in diameter but up to 2 mm in length.⁶⁸ The Si₃N₄ rods typically grow within grain volume and have random orientations.⁶⁸ The Si₃N₄ rods are insulating with a given resistivity value in the order of 10^7 Ω cm reported in reference.⁷³ Hence, the Si₃N₄ rods are not electrically active and, in most cases, are not detrimental to the performance of cast mono-like silicon solar cells.⁶⁸ The Si₃N₄ fibers are <500 nm in diameter but up to

8 mm in length.⁶⁸ The Si_3N_4 fibers grow in the grain volume and in the direction of crystallization direction. Similar to the Si_3N_4 rods, the Si_3N_4 fibers are insulating with the resistivity value in the order of $10^8 \Omega \text{ cm}$.⁶⁸ The Si_3N_4 nets are <500 nm in diameter but up to 3 mm in length.⁶⁸ The Si_3N_4 nets grow in GBs and in the direction of crystallization direction. The Si_3N_4 nets are more insulating with the resistivity value in the order of $10^{10} \Omega \text{ cm}$.⁶⁸ More information about the Si_3N_4 precipitates can be found in the references.^{68,71} Figure 19 summarizes the classification and properties of carbon and nitrogen correlated precipitates in crystalline solar silicon.

Gettering and hydrogenation are two important options to retard the detrimental effects of impurities on cast mono-like silicon solar cells. Gettering for cast mono-like silicon wafers typically includes external gettering and internal gettering. External gettering such as P-diffusion gettering, B-diffusion gettering, and poly-Si gettering can significantly reduce the concentration of metallic impurities in cast mono-like silicon. For instance, Macdonald et al.⁵⁷ reported that a P-diffusion at temperatures of $780\text{--}850^\circ\text{C}$ for 55 min in p-type deliberately contaminated Cz silicon can reduce the dissolved iron concentration to only about 3%–9% of its initial value, whereas a subsequent low temperature anneal at 650°C for 60 min can further reduce the dissolved iron concentration to around 0.1% of its initial value. Macdonald et al.⁵⁷ also claimed that B-diffusion with intact boron-rich layer (BRL) in p-type deliberately contaminated Cz silicon can getter iron impurity in silicon significantly; however, without the BRL, the effect of B-diffusion gettering is significantly reduced. The effect of various external gettering techniques can be seen in Figure 20. In

addition, Dimassi et al.⁷⁴ demonstrated that poly-Si deposition followed by a thermal annealing at 900°C for 90 min could significantly getter impurities from mc-Si, leading to an enhancement in IQE. Internal gettering at dislocation clusters is also able to enhance the electronic properties of cast mono-like silicon. Liu et al.⁷⁵ reported that internal gettering at extended defects in p-type mc-Si can greatly reduce the concentration of dissolved iron in silicon grain, and its associated mechanism is mostly due to relaxation gettering during the crystal cooling. Hydrogenation is another important option to reduce the detrimental effects of impurities in cast mono-like silicon via forming the complex with the impurities. The hydrogen-impurity complex typically is recombination inactive or has a shallow energy level and therefore can dramatically reduce the recombination activity of the impurities. For example, Liu et al.⁷⁶ reported an effective hydrogenation of interstitial iron (1% remaining) in p-type mc silicon after a thermal anneal at temperature of 700°C for 30 min. Shiraishi et al.⁷⁷ reported that hydrogen is able to passivate nickel atom to reduce its recombination activity in p-type Cz silicon.

In conclusion, impurity contamination is one of the most detrimental problems to cast mono-like silicon ingot. "Red zone," impurity decorated GBs, impurity contamination at the ingot edges are the typical problems due to impurity contamination. "Red zone," as the consequence of iron contamination, is particularly evident in cast mono-like silicon ingot, for which the detailed mechanisms are still under debate. The use of crucible with low iron content and diffusion barriers are reported to be able to suppress "red zone." Impurities also tend to precipitate in and near the sub-GBs, which enhances the

type	SiC particles	SiC filaments	Si_3N_4 rods	Si_3N_4 fibers	Si_3N_4 nets
IR microscopy					
size	1–600 μm in diameter	<5 μm in diameter, up to 3 mm in length	<30 μm in diameter, up to 2 mm in length	<500 nm in diameter, up to 8 mm in length	<500 nm in diameter, up to 3 mm in length
morphology	compact particles, frequently in clusters showing irregular surface and consisting of monocrystalline particles showing vicinal faces	irregular diameter, rough surface, multicrystalline	polygonal diameter, smooth surface, monocrystalline	steady diameter, smooth surface, monocrystalline	irregular diameter, smooth surface, multicrystalline
local growth preference	within grain volume, often at Si_3N_4 rods	mostly in grain boundaries, growing in crystallization direction	within grain volume, random orientation	within grain volume, growing in crystallization direction, branching	in grain boundaries, growing in crystallization direction
crystal structure	cubic, $\beta\text{-SiC}$	cubic, $\beta\text{-SiC}$	hexagonal, $\beta\text{-Si}_3\text{N}_4$	trigonal, $\alpha\text{-Si}_3\text{N}_4$	trigonal, $\alpha\text{-Si}_3\text{N}_4$
space group	F43m (216)	F43m (216)	P63 (173)	P31c (159)	P31c (159)
lattice constants	$a = 0.436 \text{ nm}$	$a = 0.436 \text{ nm}$	$a = 0.760 \text{ nm}$, $c = 0.291 \text{ nm}$	$a = 0.775 \text{ nm}$, $c = 0.562 \text{ nm}$	$a = 0.775 \text{ nm}$, $c = 0.562 \text{ nm}$
impurities	N, Al	N, O	Li, C, O, Mg, Ca	C, O, Ca	C, O, Al, Ca
electrical resistance	$8.17 \times 10^{-5} \Omega \text{ cm}$ (4PP)	$2 \times 10^{-3} \Omega \text{ cm}$ (4PP) [28]	$>4.7 \times 10^7 \Omega \text{ cm}$ (4PP) [28]	$(5 \pm 4) \times 10^8 \Omega \text{ cm}$ (2PP)	$(1.44 \pm 0.26) \times 10^{10} \Omega \text{ cm}$ (2PP)

FIGURE 19 Classification and properties of carbon and nitrogen correlated precipitates in crystalline solar silicon.⁶⁸ Reproduced from Richter et al.,⁶⁸ copyright 2017, Wiley-VCH Verlag

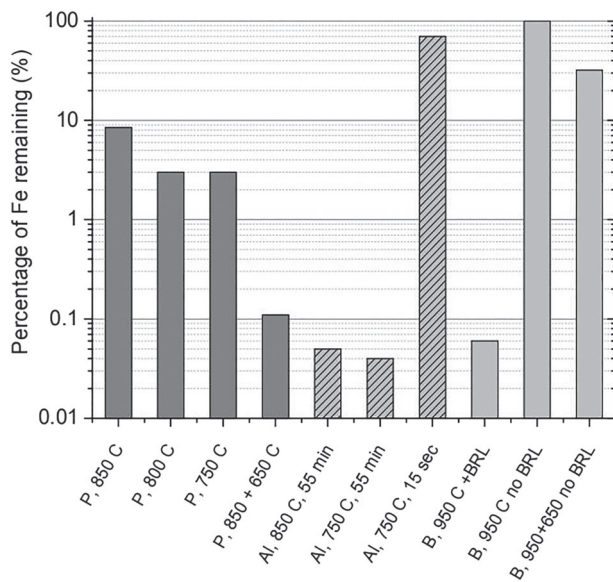


FIGURE 20 Fe gettering effectiveness for phosphorus (P)-, aluminum (Al)-, and boron (B)-diffused regions for different diffusion conditions in p-type deliberately contaminated Cz silicon.⁵⁷ Reproduced from Macdonald et al.,⁵⁷ copyright 2014, Trans Tech Publications

recombination activity of sub-GBs as well as contributes to the generation of dislocations. Impurity contamination at the ingot edges is another severe problem, but it can be suppressed by GB engineering. Light elements such as C, N, and O are other important impurities in cast mono-like silicon and play important roles on wafer quality. To reduce the detrimental effects of impurities on cast mono-like silicon, gettering and hydrogenation are two useful choices, which can dramatically reduce the concentration of interstitial impurity in silicon.

4 | LID IN CAST MONO-LIKE SILICON AND WAYS TO SUPPRESS IT

LID is a common phenomenon in silicon-based solar cells. Boron–oxygen-related defects were found to be the origin for the LID in Cz silicon. Nevertheless, cast mono-like silicon contains less oxygen content because of the characteristic of casting method and therefore boron–oxygen-related defects would not be the cause for the significant LID in cast mono-like silicon. Recently, it was reported that another LID phenomenon, called light and elevated temperature-induced degradation (LeTID), existed in mc and cast mono-like silicon. LeTID in cast mono-like silicon solar cells can cause relative power losses of over 10% relative, which is beyond the calculated scope of boron–oxygen-related defects-induced degradation. Furthermore, the time scope for LeTID is on the orders of hundreds of hours when the cast mono-like silicon was under carrier injection and at field relevant temperatures, which is much longer than the time scale of the degradation induced by boron–oxygen related defects. These are extensive studies on the behaviors of LeTID and the mechanisms associated with the

formation of LeTID, which will be discussed in the next two paragraphs in turn. At the last of this section, we will discuss the methods to suppress LeTID in terms of their advantages and shortcomings.

The behaviors of LeTID in cast mono-like silicon are similar to those in mc silicon as reported by Sio et al.,¹⁵ as both of them are grown by the almost same casting method. Therefore, in this section, we will discuss the behaviors of LeTID found in both mc and cast mono-like silicon. LeTID typically occurs under carrier injection and at elevated temperatures and will accelerate under stronger carrier injection or at higher temperatures in p-type mc-Si,⁷⁸ as shown in Figure 21. The behaviors of LeTID can be influenced by peak firing temperature, cooling rate, and annealing after the firing. In terms of peak firing temperature, Bredemeier et al.¹⁷ compared the LeTID in p-type mc-Si wafers fired at 650 and 900°C, and only observed LID in wafers fired at 900°C. Chan et al.⁷⁹ also reported that substantial LeTID could only occur in p-type mc-Si when the peak firing temperature exceeded 700°C. In terms of cooling rate, Eberle et al.¹⁹ reported that wafers of p-type mc-Si subjected to a fast-firing process with rapid cooling exhibited significantly stronger LeTID compared with the same wafers subjected to the same firing temperature, but with slower cooling rates. Sen et al.⁸⁰ further found that a slower cooling rate was only vital in the elimination of LeTID when the treatment duration time was short (1 min or less); however, with a prolonged annealing time, cooling rate no longer played an important role. In terms of annealing after the firing, Sen et al.⁸⁰ demonstrated that postfiring illuminated annealing between 350 and 500°C for a short time was able to eliminate LeTID effectively in p-type mc-Si. Nevertheless, Chan et al.⁸¹ reported that postfiring dark annealing was not able to eliminate LeTID in p-type mc-Si, but altered the subsequent degradation and regeneration rates and the degradation severity. In detail, it was found that postfiring dark annealing at temperatures of 200°C or below for a fixed time accelerated the degradation and subsequent regeneration rates and the degradation severity, whereas at

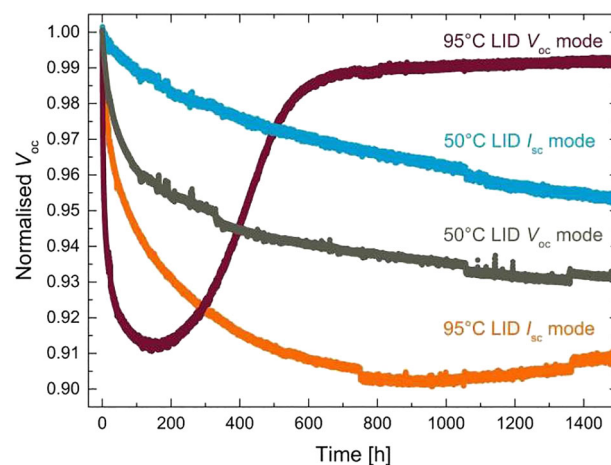


FIGURE 21 The behaviors of light and elevated temperature-induced degradation in p-type mc-Si at various temperatures and under operation conditions.⁷⁸ Reproduced from Kersten,⁷⁸ copyright 2015, IEEE

higher temperatures it appeared that a second defect with a dramatically longer degradation and regeneration rates emerged. This phenomenon is shown in Figure 22.

The mechanisms associated with the formation of LeTID were also extensively studied. So far, hydrogen and metallic impurities are generally considered to play an important role on the formation of LeTID in mc and cast mono-like silicon. On one hand, Vargas et al.⁸² found a correlation between the amounts of hydrogen released from the dielectric layer during firing and the extent of the degradation in p-type mc-Si, as shown in Figure 23, and therefore suggested that hydrogen was involved in the formation of LeTID. Eberle et al.¹⁹ reported that low peak firing temperature and slow cooling rate could suppress LeTID in p-type mc-Si, which was consistent with the behavior of hydrogen in silicon. Therefore, they suggested that hydrogen might play a role on the formation of LeTID. Moreover, Nakayashiki et al.,⁸³ Morishige et al.,⁸⁴ Bredemeier et al.,¹⁷ Jensen et al.,²¹ Varshney et al.,⁸⁵ and Chan et al.⁸¹ all hypothesized that hydrogen played a key role on the formation of LeTID. On the other hand, other researchers pointed out that metallic impurity might be a candidate on the formation of LeTID. Nakayashiki et al.⁸⁶ analyzed the lifetime spectroscopy of the degraded state of LeTID in p-type mc-Si and found that the defect had an asymmetry ratio of electron to hole capture cross sections at ~ 28.5 , which was most consistent with molybdenum (Mo), tungsten (W), and titanium (Ti). Morishige et al.⁸⁴ reported that the responsible defect in the degraded state of LeTID in p-type mc-Si had an energy level between 0.3 and 0.7 eV above the

valence band and a capture cross section ratio between 26 and 36 via the lifetime spectroscopy analysis, as shown in Figure 24, and therefore suggested a deep-level donor point defect, such as metallic impurity, for causing LeTID. Furthermore, Both Bredemeier et al.⁸⁷ and Jensen et al.²¹ claimed a defect model for explaining LeTID that metal precipitates dissolved during firing, and then the mobile metal atoms bonded to a homogeneously distributed impurity, and subsequently the defect complex dissociated during elevated temperature and illumination. It should be noted that the model of hydrogen and the model of metallic impurity are not necessary to contradict with each other and are possible to play a role simultaneously.

The methods to suppress LeTID have been intensely studied. So far, lower peak firing temperature,⁸⁴ modification of firing profile (slower cooling rate),¹⁹ thin-film barrier layer,⁸⁵ controlling starting material quality,^{86,88} accelerated degradation and regeneration,⁸⁴ and design of high-temperature steps to alter impurity distributions^{20,89} have been reported to suppress LeTID effectively. Nevertheless, the advantages and disadvantages of these methods should be discussed. Lower peak firing temperature is able to mitigate LeTID completely in p-type mc-Si; however, it is not compatible with the metallization process that requires a high peak firing temperature at around 800°C. Modification of firing profile with slower cooling rate will reduce the performance of hydrogen passivation⁹⁰ as well as the yield. The addition of atomic layer deposition grown AlO_x layer will add the complexity of fabrication processes. Controlling starting material quality is compatible with fabrication processes; however, it adds cost of the

FIGURE 22 A, Relative change in V_{oc} of p-type mc-Si solar cells during light soaking that underwent an initial dark annealing at various temperatures for 2.5 h. B, Same with log scale. The light soaking was conducted at 75°C and under 1000 W/m² illumination intensity.⁸¹ Reproduced from Chan et al.,⁸¹ copyright 2017, WILEY-VCH Verlag GmbH & Co. KGaA, Weinheim

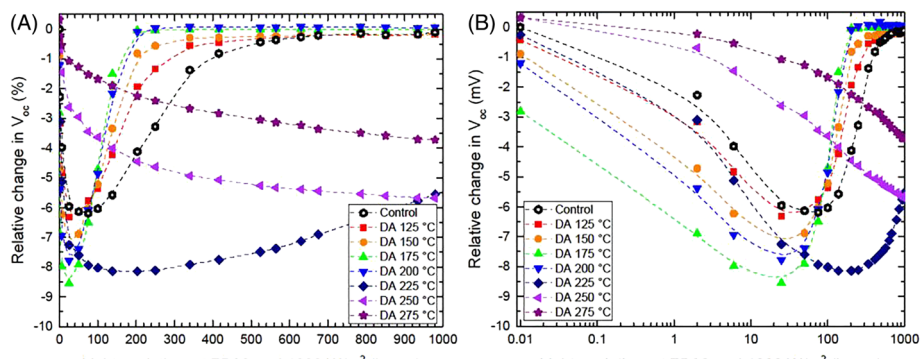
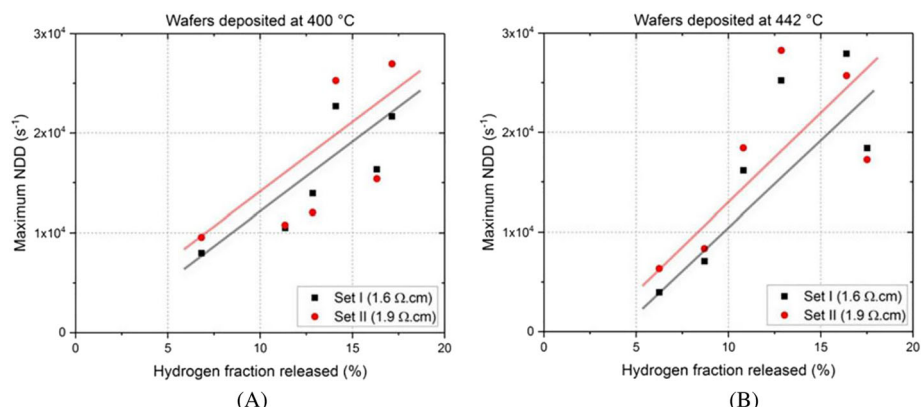


FIGURE 23 Maximum normalized defect density (NDD) as a function of the hydrogen fraction released during the deposition process in p-type mc-Si.⁸² (A) The deposition temperature was 400°C and (B) the deposition temperature was 442°C. Reproduced from Vargas et al.,⁸² copyright 2018, IEEE



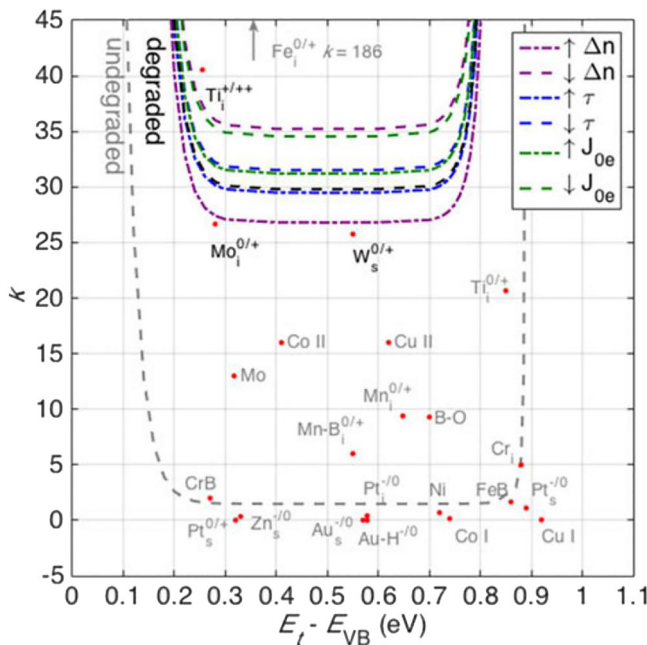


FIGURE 24 Capture cross section ratio k as a function of energy level E_t above the valence band for the defect responsible for LeTID in the degraded state (black curve) and undegraded state (gray curve) in p-type mc-Si.⁸⁴ Reproduced from Morishige et al.,⁸⁴ copyright 2016, IEEE

wafers. Accelerated degradation and regeneration are an easy method to operate; however, the complete passivation and long-term stability have not been achieved.^{25,91} Design of high-temperature steps to alter impurity distributions, such as gettering, can both reduce the extent of LeTID and increase the lifetime of the wafers; however, it increases the thermal budget of the fabrication processes. All the methods mentioned above have some limitations, a further improvement of the method will require deeper understanding of the defect responsible for LeTID.

In conclusion, LeTID is able to cause power loss of cast mono-like silicon solar cells over 10% relative and will take a decade to recover in the field condition,¹⁶ which significantly reduce the power output of cast mono-like silicon modules. The behaviors of LeTID have been intensely studied and found to depend on various parameters such as peak firing temperature and cooling rate. The mechanisms associated with the formation of LeTID are hypothesized to be related to the model of hydrogen or the model of metallic impurity or both of them;

however, the root cause of LeTID has not yet been understood. The methods to suppress LeTID can be several, including modification of firing temperature or profile, accelerated degradation and regeneration and et al. Nevertheless, these methods still have some limitations, and a further improvement of the methods will require deeper understanding of the root cause of LeTID.

5 | CELL EFFICIENCY POTENTIAL OF CAST MONO-LIKE SILICON

Cast mono-like silicon solar cells can achieve much higher efficiency than mc silicon solar cells, which is even close to the efficiency performance of Cz silicon solar cells.⁹² For instance, Y. Lv et al.³ reported that PERC solar cells prepared from p-type cast mono-like silicon wafers are able to achieve an average efficiency of 22.2%, which is slightly lower than the Cz monocrystalline silicon counterparts at 22.8% for PERC structure. Moreover, cast mono-like silicon is grown by casting method, and therefore, its cost is much cheaper than Cz silicon. Nevertheless, cast mono-like silicon often suffers from dislocations, sub-GBs, multicrystallization, and impurity contamination, which cause a wide efficiency distribution of cast mono-like silicon solar cells with a long low-efficiency tail.⁹² As dislocations and sub-GBs propagate and multiply from seeds to the top of the ingot, cast mono-like silicon wafers from the bottom of the ingot (above the “red zone”) generally have relative higher minority carrier lifetime. Moreover, the minority carrier lifetime decreases with the increasing height toward the top of the ingot. Some studies were done to overcome the low-efficiency tail of cast mono-like silicon solar cells, including the modification of crystal growth orientation⁵⁶ and functional GBs.⁶ In addition, cast mono-like silicon wafers can be used as the base material for high-efficiency cell structure. In this section, we will introduce the characteristics of conventional cast mono-like silicon solar cells, the methods to improve average efficiency of cast mono-like silicon solar cells, and high-efficiency cell structure with cast mono-like silicon as the base material in turn.

The characteristics of cast mono-like silicon solar cells depend on the wafer position and the wafer type. Gong et al.⁹³ demonstrated the BSF cell efficiency distribution of p-type cast mono-like silicon solar cells from a whole ingot and found a non-normal distribution with a long tail on the low-efficiency side, as shown in Figure 25A. They further correlate the efficiency distribution with the position of

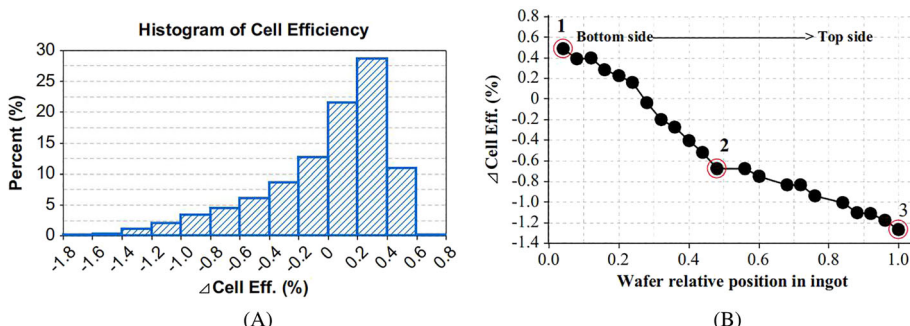


FIGURE 25 (A) Histogram of back surface field cell efficiency of the whole wafers from one p-type cast mono-like silicon ingot and (B) cell efficiency trend diagram relative to wafer position in one p-type cast mono-like silicon ingot.⁹³ Reproduced from Gong et al.,⁹³ copyright 2014, Elsevier B.V

silicon wafer in the block and found that efficiency drops almost linearly from bottom to top, as shown in Figure 25B. Sio et al.⁹⁴ reported that n-type cast mono-like silicon solar cells have relatively high efficiency than that of p-type cast mono-like silicon solar cells, because of that n-type cast mono-like silicon wafers are less affected by dislocation clusters and intra-grain recombination.

The methods to improve the average efficiency of cast mono-like silicon solar cells include functional GBs and appropriate surface texturing. Zhang et al.⁶ reported that functional $\Sigma 13$ GBs at seed junctions can effectively suppress dislocation generation and result in an average efficiency of 20.1%. Gu et al.⁴² reported that alkaline texturing on cast mono-like silicon surface can lead to lower reflectance compared with that by acidic texturing and a similar IQE. As a consequence, the cast mono-like silicon solar cells employing alkaline texturing typically have higher efficiency than that employing acidic texturing. Figure 26 reveals the pictures, the measured reflectance, the IQE, and the efficiency of four kinds of silicon solar cells employing alkaline or acidic texturing.

Cast mono-like silicon can also be used as the substrate material for high-efficiency solar cell structure. Frey et al.⁹⁵ made large area (243.36 cm^2) back-junction passivated emitter rear totally diffused silicon solar cells with efficiency of 20.2% using n type cast mono-like silicon as substrate. Recently, Y. Lv et al.³ demonstrated that large-area screen-printed PERC solar cells based on p-type cast mono-like silicon

can achieve a maximum efficiency of 22.5% and an average efficiency of 22.2% via the use of the techniques such as selective emitter (SE) and triple-SiN_x:H layers. The above results indicate that cast mono-like silicon wafers can be compatible with current cell technology to achieve high efficiency. Cast mono-like silicon wafers also have the compatibility with last generations of high-efficiency solar cells. For instance, Jay et al.⁹⁶ demonstrated that large-area n-type a-Si:H/c-Si heterojunction solar cells using cast mono-like silicon wafers as substrate can achieve efficiency over 21.5%, of which the I-V curve is shown in Figure 27. Kivambe et al.⁹⁷ also reported a record efficiency of 22.58% and 22.15% for n-type and p-type cast mono-like silicon-based hetero-junction solar cells on small area, respectively. It is worth noting that the n-type and p-type cast mono-like silicon wafers were P-diffusion gettered before cell fabrication processes, and therefore, the wafer quality was much improved for the record heterojunction solar cells. Recently, Trina Solar reported a conversion efficiency record of 23.22% for a TOPCon-like solar cell based on an n-type cast mono-like silicon wafer. However, it is not published in the literature up to date.

In conclusion, cast mono-like silicon solar cells can achieve higher efficiency than that of mc silicon solar cells; however, cast mono-like silicon solar cells have a non-normal efficiency distribution with a long tail on the low-efficiency side because of the problems of dislocation clusters, "red zone" and multicrystallization. Several methods have

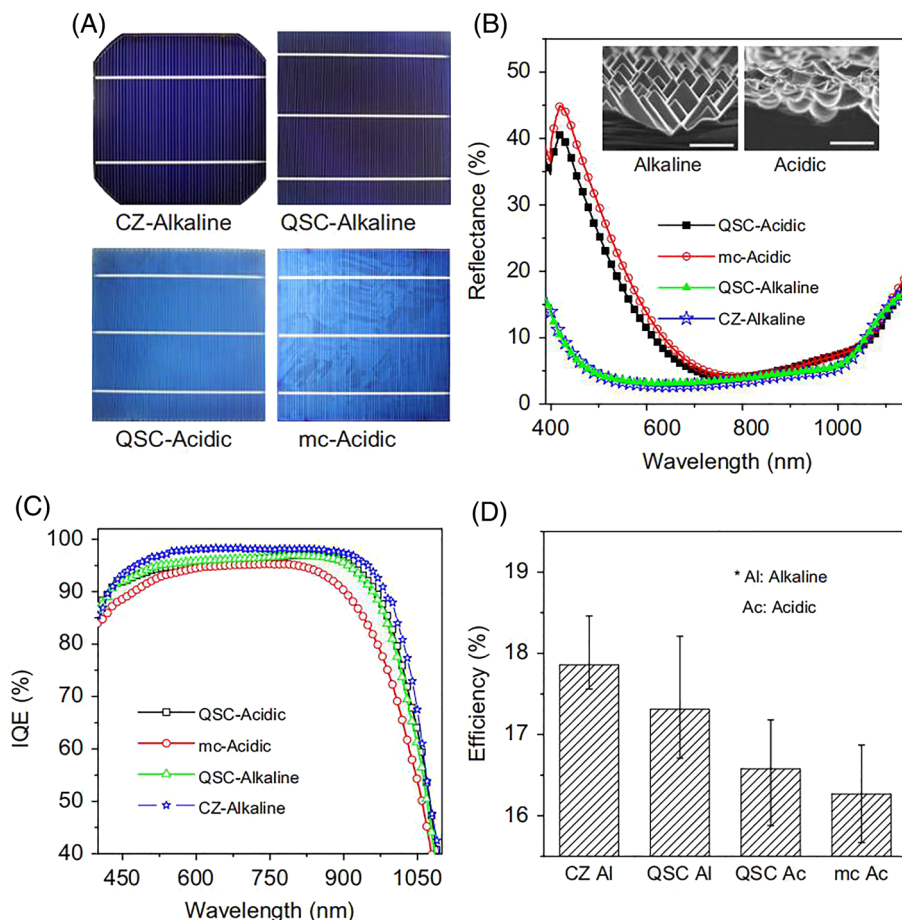


FIGURE 26 (A) The pictures, (B) the measured reflectance, (C) the IQE, and (D) the efficiency of four kinds of silicon solar cells (Cz, cast mono-like, multicrystalline) using alkaline or acidic texturing.⁴² Reproduced from Xin et al.,⁴² copyright 2012, Elsevier B.V.

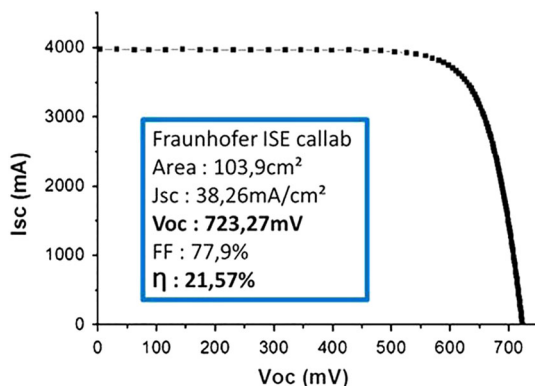


FIGURE 27 I-V curve of the heterojunction silicon solar cell at AM1.5 certified by Fraunhofer ISE Callab.⁹⁶ Reproduced from Jay et al.,⁹⁶ copyright 2014, Elsevier B.V

been reported to improve the average efficiency of cast mono-like silicon solar cells, including functional GBs and appropriate surface texturing. Furthermore, cast mono-like silicon is demonstrated to be a promising substrate for high-efficiency silicon solar cell structure.

6 | CONCLUSION AND FUTURE PROSPECT

In this overview, we review the-state-of-the-art knowledge of cast mono-like silicon technique, including the growth method and conditions, the dominant defects, LID, and cell efficiency potential. In terms of the growth method and conditions, cast mono-like silicon is generally grown by directional solidification and its quality can be influenced by temperature profile in the furnace, the m-c interface, and seed arrangements. In brief, a small temperature gradient across the m-c interface is reported to be good for reducing the thermal stresses in the grown ingot. The m-c interface is better to be slightly convex in relation to the melt. Last, one single large seed is found to be able to suppress dislocation generation; however, very large seed for industrial size crucible is impossible because of the technical limitation of the size of Cz silicon seed.

The dominant defects in cast mono-like silicon consist of multicrystallization, dislocations, sub-GBs, and impurity contamination. Multicrystallization refers to the phenomenon that various grains with a different crystallographic orientation nucleate at random sites on the inner side walls of the crucible and then extend directionally inside the ingot. Multicrystallization can cause a significant reduction in power conversion efficiency, and therefore, it is crucial to mitigate it. Careful control of the temperature profile and the m-c interface can assist in suppressing multicrystallization, nevertheless, it may not be compatible with the best growth conditions. Functional GBs are also able to mitigate multicrystallization and have the advantage that it can be applied to a wide range of growth conditions. Dislocations are the dominant lifetime killer in the cast mono-like silicon. Dislocations typically generate from the GBs formed at the seed joints and then propagate and multiply along the growth direction. The

mechanisms of dislocation generation are extensively studied and these studies focus on two types of investigations: the influence of the GB microstructure and the influence of the stress distribution. Dislocations generated from small angle and CSL GBs are sensitive to the microstructure of the GBs. For instance, it was found that $\sim 0^\circ$ -tilt GBs generated dislocations more easily than large-angle tilt GBs during the crystal growth. On the other hand, dislocations generated from a random GB are sensitive to the stress around the GBs. Studies reported that dislocations generated from a random GB demonstrated a positive correlation with the shear stress around the GB. The methods to suppress dislocation generation and propagation are also extensively studied, including special GBs, functional defects, different crystal orientations, and seed partitions. These methods are effective; however, further improvement is still needed to completely mitigate dislocation generation or propagation. Sub-GBs often appear simultaneously with dislocations. The origin of sub-GBs can be indentation damage on seed surface or seed joints. Once sub-GBs are formed, they will be the origin of dislocation generation and the sink for the impurity precipitation. Sub-GBs can be mitigated by the careful alignment of seeds so as to minimize the misorientation angle and by a before-cast preparation of the feedstock to avoid the sharp points. Like the mc silicon, impurity contamination is severe in cast mono-like silicon. “Red zone” is one of the mostly detrimental effects of impurity contamination. “Red zone” refers to the low carrier lifetime zone at the bottom of cast mono-like silicon ingot and it can be twice as wide as that found in conventional cast mc silicon. The formation of the “red zone” is attributed to the high concentration of iron impurities diffusing from the quartz crucible, nevertheless, the detailed mechanisms are still under debate. The methods to suppress “red zone” can be several, including a reduction in duration time before crystal growth and the use of iron diffusion barriers. Except for the problem of “red zone,” impurities can also decorate the GBs to enhance their recombination activities. Functional defects are reported to be able to getter impurity and meanwhile become barriers for impurity in-diffusion. In addition, the use of crucible with low impurity content can also suppress impurity contamination in cast mono-like silicon.

LID in cast mono-like silicon typically occurs under carrier injection and at elevated temperatures and can cause power loss over 10% relative. The behaviors of the LID in cast mono-like silicon are similar to those in mc silicon, which are extensively studied. So far, it has been found that the behaviors of the LID can be influenced by peak firing temperature, cooling rate, and annealing after the firing. The mechanisms associated with the formation of the LID were also extensively studied. Hydrogen and metallic impurities are generally considered to play an important role on the formation of the LID in mc and cast mono-like silicon. Based on the understanding of the LID, several methods were proposed to mitigate LID, which include lower peak firing temperature, modification of firing profile (slower cooling rate), thin-film barrier layer, controlling starting material quality, accelerated degradation, and regeneration and design of high-temperature steps to alter impurity distributions. These methods have their own advantages and limitations, and therefore, further improvement will require deeper understanding of the mechanisms of the LID.

So far, cast mono-like silicon solar cells have demonstrated higher efficiency potential than conventional mc silicon solar cells. Nevertheless, cast mono-like silicon solar cells suffer from a variety of problems, such as multicrystallization, dislocations, sub-GBs, and impurity contamination and therefore have a non-normal efficiency distribution with a long tail on the low-efficiency side. Functional GBs and appropriate surface texturing are reported to be able to enhance the average efficiency of cast mono-like silicon solar cells. Furthermore, it is demonstrated that cast mono-like silicon can be used as the base material for high-efficiency solar cell structure.

In the future, more studies are required to understand the mechanisms of the defects generation and propagation as well as the origin of the LID in cast mono-like silicon. With the prolonged efforts on improving cast mono-like silicon technique, it is feasible that cast mono-like silicon will become the dominant material for next-generation silicon solar cells.

ACKNOWLEDGEMENTS

The authors would like to thank the National Natural Science Foundation of China (Nos. 51602085, 51532007, and 61974129) and the National Key Research and Development Project (2018YFB1500401) for financial support.

CONFLICT OF INTEREST

The authors declare no conflict of interest.

ORCID

Lihui Song  <https://orcid.org/0000-0001-5536-8388>
 Xuegong Yu  <https://orcid.org/0000-0002-0354-8501>

REFERENCES

- Jouini A, Ponthenier D, Lignier H, Enjalbert N, Camel D. Improved multicrystalline silicon ingot crystal quality through seed growth for high efficiency solar cells. *Prog Photovolt Res Appl.* 2012;20:735-746.
- Gao B, Nakano S, Harada H, Miyamura Y, Sekiguchi T, Kakimoto K. Reduction of polycrystalline grains region near the crucible wall during seeded growth of monocrystalline silicon in a unidirectional solidification furnace. *J Cryst Growth.* 2012;352:47-52.
- Lv Y, Zhuang YF, Wang WJ, et al. Towards high-efficiency industrial p-type mono-like Si PERC solar cells. *Solar Energy Mater Solar Cells.* 2020;204:1-9, 110202. <https://doi.org/10.1016/j.solmat.2019.110202>
- Kutsukake K, Usami N, Ohno Y, Tokumoto Y, Yonenaga I. Mono-like silicon growth using functional grain boundaries to limit area of multicrystalline grains. *IEEE J Photovolt.* 2013;4:84-87.
- Tsoutsouva MG, Oliveira VA, Camel D, Baruchel J, Marie B, Lafford TA. Mono-like silicon ingots grown on low angle misoriented seeds: defect characterization by synchrotron X-ray diffraction imaging. *Acta Mater.* 2015;88:112-120.
- Zhang F, Yu X, Liu C, et al. Designing functional Σ 13 grain boundaries at seed junctions for high-quality cast quasi-single crystalline silicon. *Solar Energy Mater Solar Cells.* 2019;200:1-7, 109985. <https://doi.org/10.1016/j.solmat.2019.109985>
- Trempa M, Reimann C, Friedrich J, Müller G, Richter T. Influence of grain boundaries intentionally induced between seed plates on the defect generation in quasi-mono-crystalline silicon ingots. *Crystal Res Technol.* 2015;50:124-132.
- Hu D, Yuan S, He L, et al. Higher quality mono-like cast silicon with induced grain boundaries. *Solar Energy Mater Solar Cells.* 2015;140: 121-125.
- Wu YC, Lan A, Yang CF, et al. The effect of seed arrangements on the quality of n-type mono-like silicon grown by directional solidification. *Cryst Growth Des.* 2016;16(11):6641-6647.
- Bing G, Nakano S, Kakimoto K. Influence of back-diffusion of iron impurity on lifetime distribution near the seed-crystal interface in seed cast-grown monocrystalline silicon by numerical modeling. *Cryst Growth Des.* 2011;12:522-525.
- Yu X, Xin G, Shuai Y, Guo K, Yang D. Two-peak characteristic distribution of iron impurities at the bottom of cast quasi-single-crystalline silicon ingot. *Scr Mater.* 2013;68:655-657.
- Istratov AA, Hieslmair H, Weber ER. Iron contamination in silicon technology. *Applied Physics a.* 2000;70:489-534.
- Trempa M, Reimann C, Friedrich J, et al. Investigation of iron contamination of seed crystals and its impact on lifetime distribution in Quasimono silicon ingots. *J Cryst Growth.* 2015;429:56-62.
- Hu D, Yuan S, Yu X, et al. Grain boundary engineering of high performance multicrystalline silicon: control of iron contamination at the ingot edge. *Solar Energy Mater Solar Cells.* 2017;171:131-135.
- Sio HC, Wang H, Wang Q, et al. Light and elevated temperature induced degradation in p-type and n-type cast-grown multicrystalline and mono-like silicon. *Solar Energy Mater Solar Cells.* 2018;182:98-104. <https://doi.org/10.1016/j.solmat.2018.03.002>
- Kersten F, Engelhart P, Ploigt HC, et al. Degradation of multicrystalline silicon solar cells and modules after illumination at elevated temperature. *Solar Energy Mater Solar Cells.* 2015;142:83-86.
- Bredemeier D, Walter D, Herlufsen S, Schmidt J. Lifetime degradation and regeneration in multicrystalline silicon under illumination at elevated temperature. *Aip Advances.* 2016;6:1-8, 861.
- Chan CE, Payne DNR, Hallam BJ, Abbott MD, Wenham SR. Rapid stabilization of high-performance multicrystalline P-type silicon PERC cells. *IEEE J Photovolt.* 2017;6:1473-1479.
- Eberle R, Kwapił W, Schindler F, Schubert MC, Glunz SW. Impact of the firing temperature profile on light induced degradation of multicrystalline silicon. *Phys Status Solidi Rapid Res Lett.* 2016;10: n/a-n/a.
- Zuschlag A, Skorka D, Hahn G. Degradation and regeneration in mc-Si after different gettering steps: degradation and regeneration in mc-Si. *Prog Photovolt Res Appl.* 2016;25(7):545-552.
- Jensen MA, Morishige AE, Hofstetter J, Needleman DB, Buonassisi T. Evolution of LeTID defects in p-type multicrystalline silicon during degradation and regeneration. *IEEE J Photovolt.* 2017;7:980-987.
- Vargas C, Kim K, Coletti G, et al. Carrier-induced degradation in multicrystalline silicon: dependence on the silicon nitride passivation layer and hydrogen released during firing. *IEEE J Photovolt.* 2018;1-8.
- Buonassisi T, Istratov AA, Pickett MD, et al. Chemical natures and distributions of metal impurities in multicrystalline silicon materials. *Prog Photovolt Res Appl.* 2010;14:513-531.
- Jensen MA, Morishige AE, Hofstetter J, Needleman DB, Buonassisi T. Evolution of LeTID defects in p-type multicrystalline silicon during degradation and regeneration. *IEEE J Photovolt.* 2017;1-8.
- Payne DNR, Chan CE, Hallam BJ, et al. Acceleration and mitigation of carrier-induced degradation in p-type multi-crystalline silicon. *Physica Status Solidi (RRL) - Rapid Res Lett.* 2016;10(3):237-241.
- Hallam BJ, Hamer PG, Wenham SR, Abbott MD, Einhaus R. Advanced bulk defect passivation for silicon solar cells. *IEEE J Photovolt.* 2013;4: 88-95.
- Wang P, Cui C, Yang D, Yu X. Seed-assisted growth of cast-mono silicon for photovoltaic application: challenges and strategies. *Solar RRL.* 2020;4:1-20, 1900486.
- Kutsukake K. In: Yang D, ed. *Handbook of Photovoltaic Silicon.* Berlin Heidelberg: Springer; 2018:1-20.

29. Li Z, Liu L, Ma W, Liu L, Kakimoto K. Effects of argon flow on heat transfer in a directional solidification process for silicon solar cells. *J Cryst Growth.* 2011;318:298-303.
30. Miyazawa H, Liu L, Hisamatsu S, Kakimoto K. Numerical analysis of the influence of tilt of crucibles on interface shape and fields of temperature and velocity in the unidirectional solidification process. *J Cryst Growth.* 2008;310:1034-1039.
31. Miyazawa H, Liu L, Kakimoto K. Numerical analysis of influence of crucible shape on interface shape in a unidirectional solidification process. *J Cryst Growth.* 2008;310:1142-1147.
32. Xu M, Zheng L, Zhang H, Zhao B, Wang C, Xu F. Thermal system design and optimization of an industrial silicon directional solidification system. *J Cryst Growth.* 2011;318:288-292.
33. Liu LJ, Nakano S, Kakimoto K. Dynamic simulation of temperature and iron distributions in a casting process for crystalline silicon solar cells with a global model. *J Cryst Growth.* 2006;292:515-518.
34. Yang X, Ma W, Lv G, et al. Effect of heat transfer during the vacuum directional solidification process on the crystal quality of multicrystalline silicon. *Metallurgical Mater Trans E.* 2015;2(1):39-49.
35. Chen XJ, Nakano S, Liu LJ, Kakimoto K. Study on thermal stress in a silicon ingot during a unidirectional solidification process. *J Cryst Growth.* 2008;310:4330-4335.
36. Li Z, Liu L, Xin L, Zhang Y, Xiong J. Effects of argon flow on melt convection and interface shape in a directional solidification process for an industrial-size solar silicon ingot. *J Cryst Growth.* 2012;360:87-91.
37. Li Z, Liu L, Ma W, Zan Z. in International Conference on Materials for Renewable Energy & Environment.
38. Hu C, Chen JC, Nguyen TH, et al. Optimization of heat transfer during the directional solidification process of 1600 kg silicon feedstock. *J Cryst Growth.* 2018;484:70-77.
39. Teng YY, Chen JC, Huang BS, Chang CH. Numerical simulation of impurity transport under the effect of a gas flow guidance device during the growth of multicrystalline silicon ingots by the directional solidification process. *J Cryst Growth.* 2014;385:1-8.
40. Camel D, Cayron C, Barou F, et al. in 29th European Photovoltaic Solar Energy Conference and Exhibition. 793-797.
41. Miyamura Y, Harada H, Jiptner K, et al. Crystal growth of 50 cm square mono-like Si by directional solidification and its characterization. *J Cryst Growth.* 2014;401:133-136.
42. Xin GU, Yu X, Guo K, Chen L, Wang D, Yang D. Seed-assisted cast quasi-single crystalline silicon for photovoltaic application: towards high efficiency and low cost silicon solar cells. *Solar Energy Mater Solar Cells.* 2012;101:95-101.
43. Liu L, Yu Q, Qi X, Zhao W, Zhong G. Controlling solidification front shape and thermal stress in growing quasi-single-crystal silicon ingots: process design for seeded directional solidification. *Appl Therm Eng.* 2015;91:225-233.
44. Ekstrøm KE, Stokkan G, Søndenå R, Dalaker H, Sabatino MD. Structure and dislocation development in mono-like silicon. *Physica Status Solidi.* 2015;212:2278-2288.
45. Trempa M, Reimann C, Friedrich J, et al. Defect formation induced by seed-joints during directional solidification of quasi-mono-crystalline silicon ingots. *J Cryst Growth.* 2014;405:131-141.
46. Takahashi I, Usami N, Kutsukake K, Stokkan G, Morishita K, Nakajima K. Generation mechanism of dislocations during directional solidification of multicrystalline silicon using artificially designed seed. *J Cryst Growth.* 2010;312(7):897-901.
47. Usami N, Yokoyama R, Takahashi I, Kutsukake K, Nakajima K. Relationship between grain boundary structures in Si multicrystals and generation of dislocations during crystal growth. *J Appl Phys.* 2010; 107(347):1-5, 013511.
48. Lan CY, Wu YC, Lan A, et al. Control of ingot quality and solar cell appearance of cast mono-like silicon by using seed partitions. *J Cryst Growth.* 2017;475:136-143.
49. Takahashi I, Joonwichien S, Iwata T, Usami N. Seed manipulation for artificially controlled defect technique in new growth method for quasi-monocrystalline Si ingot based on casting. *Applied Physics Express.* 2015;8:1-4, 105501.
50. Divgalpitiya WR, Morrison SR, Vercruyse G, Praet A, Gomes WP. Hydrogen passivation of dislocations in silicon. *Solar Energy Mater.* 1987;15:141-151.
51. Martinuzzi S, Périchaud I, Warchol FO. Hydrogen passivation of defects in multicrystalline silicon solar cells. *Solar Energy Mater Solar Cells.* 2003;80:343-353.
52. Song L, Wenham A, Wang S, et al. Laser enhanced hydrogen passivation of silicon wafers. *Int J Photoenergy.* 2015;2015:1-13.
53. Tsoutsouva MG, Oliveira VA, Camel D, et al. Segregation, precipitation and dislocation generation between seeds in directionally solidified mono-like silicon for photovoltaic applications. *J Cryst Growth.* 2014;401:397-403.
54. Ryningen B, Stokkan G, Kivambe M, Ervik T, Lohne O. Growth of dislocation clusters during directional solidification of multicrystalline silicon ingots. *Acta Mater.* 2011;59:7703-7710.
55. Moralejo B, Tejero A, Hortelano V, Martínez O, Jiménez J, Parra V. Electrical and optical characterization of extended defects in silicon mono-cast material. *Physica Status Solidi.* 2012;9:2158-2163.
56. Zhang F, Yu X, Hu D, et al. Controlling dislocation gliding and propagation in quasi-single crystalline silicon by using <110>-oriented seeds. *Solar Energy Mater Solar Cells.* 2019;193:214-218. <https://doi.org/10.1016/j.solmat.2019.01.026>
57. Macdonald D, Liu A, Phang SP. External and internal gettering of interstitial iron in silicon for solar cells. *Solid State Phenomena.* 2013; 205-206:26-33.
58. Bing G, Nakano S, Kakimoto K. Influence of back-diffusion of iron impurity on lifetime distribution near the seed-crystal interface in seed cast-grown monocrystalline silicon by numerical modeling. *Cryst Growth Des.* 2016;12:522-525.
59. Ohno Y, Kutsukake K, Deura M, et al. Recombination activity of nickel, copper, and oxygen atoms segregating at grain boundaries in mono-like silicon crystals. *Appl Phys Lett.* 2016;109(676):1-4, 142105.
60. Hayama Y, Takahashi I, Usami N. Controlling impurity distributions in crystalline Si for solar cells by using artificial designed defects. *J Cryst Growth.* 2016;468:610-613, S0022024816309617.
61. Breitenstein O, Bauer J, Bothe K, et al. Understanding junction breakdown in multicrystalline solar cells. *J Appl Phys.* 2011;109(7):1-10, 071101.
62. Bauer J, Wagner JM, Lotnyk A, et al. Hot spots in multicrystalline silicon solar cells: avalanche breakdown due to etch pits. *Phys Status Solidi-Rapid Res Lett.* 2009;3(2-3):40-42.
63. Kissinger G. *Oxygen Impurity in Crystalline Silicon.* Spring Nature; 2019.
64. Murin LI, Markevich VP. Materials Science Forum 1995.
65. Lerouelle J. Influence of carbon on oxygen behavior in silicon. *Physica Status Solidi.* 2010;67:177-181.
66. Kakimoto BGK. *Carbon Impurity in Crystalline Silicon.* Spring Nature; 2019.
67. Kakimoto BGK. In: Yang D, ed. *Handbook of Photovoltaic Silicon.* Spring Nature; 2017.
68. Richter S, Bauer J, Breitenstein O. Growth of carbon and nitrogen containing precipitates in crystalline solar silicon and their influence on solar cells. *Phys Status Solidi Rapid Res Lett.* 2017;11(2):1-17, 1600354.
69. Möller HJ, Funke C, Bauer J, Köstner S, Straube H, Breitenstein O. *Growth of Silicon Carbide Filaments in Multicrystalline Silicon for Solar Cells.* Trans Tech Publications Ltd; 2015.
70. Rao H, Bates HE, Ravi KV. Electrical effects of SiC inclusions in EFG silicon ribbon solar cells. *J Appl Phys.* 1976;47:2614-2619.

71. Yang SYD. *Nitrogen Impurity in Crystalline Silicon*. Spring Nature; 2019.
72. Yang DR, Yu X. in Defect & Diffusion Forum
73. Bauer J, Breitenstein O, Rakotoniaina JP. Electronic activity of SiC precipitates in multicrystalline solar silicon. *Physica Status Solidi*. 2010;204:2190-2195.
74. Dimassi W, Bouaicha M, Kharroubi M, Lajnef M, Ezzaouia H, Bessaïs B. Two-dimensional LBIC and internal quantum efficiency investigations of porous silicon-based gettering procedure in multicrystalline silicon. *Solar Energy Mater Solar Cells*. 2008;92(11):1421-1424.
75. Liu AY, Walter D, Phang SP, Macdonald D. Investigating internal gettering of iron at grain boundaries in multicrystalline silicon via photoluminescence imaging. *IEEE J Photovolt*. 2012;2:479-484.
76. Liu AY, Sun C, Macdonald D. Hydrogen passivation of interstitial iron in boron-doped multicrystalline silicon during annealing. *J Appl Phys*. 2014;116:489-534.
77. Shiraishi M, Sachse JU, Lemke H, Weber J. DLTS analysis of nickel-hydrogen complex defects in silicon. *Mater Sci Eng B-Adv Funct Solid-State Mater*. 1999;58:130-133.
78. Kersten F, Engelhart P, Ploigt HC, et al. A new mc-Si degradation effect called LeTID[C]// Photovoltaic Specialist Conference. *IEEE*, 2015.
79. Chan CE, Payne DNR, Hallam BJ, Abbott MD, Wenham SR. Rapid stabilization of high-performance multicrystalline P-type silicon PERC cells. *IEEE J Photovolt*. 2016;1:1-7.
80. Sen C, Kim M, Chen D, et al. Assessing the impact of thermal profiles on the elimination of light- and elevated-temperature-induced degradation. *IEEE J Photovolt*. 2018;9:40-48.
81. Chan C, Fung TH, Abbott M, et al. Modulation of carrier-induced defect kinetics in multi-crystalline silicon PERC cells through dark annealing. *Solar Rrl*. 2017;1(2):1-5, 1600028.
82. Vargas C, Kim K, Coletti G, et al. Carrier-induced degradation in multicrystalline silicon: dependence on the silicon nitride passivation layer and hydrogen released during firing. *IEEE J Photovolt*. 2018;8(2):413-420.
83. Nakayashiki K, Hofstetter J, Morishige AE, Li TTA, Buonassisi T. Engineering solutions and root-cause analysis for light-induced degradation in p-type multicrystalline silicon PERC modules. *IEEE J Photovolt*. 2016;6:1-9.
84. Morishige AE, Jensen MA, Needleman DB, et al. Lifetime spectroscopy investigation of light-induced degradation in p-type multicrystalline silicon PERC. *IEEE J Photovolt*. 2016;6(6):1466-1472.
85. Varshney U, Hallam B, Hamer P, et al. Controlling light- and elevated-temperature-induced degradation with thin film barrier layers. *IEEE J Photovolt*. 2019;10(1):1-9. <https://doi.org/10.1109/JPHOTOV.2019.2945199>
86. Nakayashiki K, Hofstetter J, Morishige AE, Li TTA, Buonassisi T. Engineering solutions and root-cause analysis for light-induced degradation in p-type multicrystalline silicon PERC modules. *IEEE J Photovolt*. 2017;6:860-868.
87. Bredemeier D, Walter D, Herlufsen S, Schmidt J. Understanding the light-induced lifetime degradation and regeneration in multicrystalline silicon. *Energy Procedia*. 2016;92:773-778.
88. Ramspeck K, Zimmermann S, Nagel H, Metz A, Seidl A. in Proc. 27th Eur. Photovolt. Sol. Energy Conf. Exhib. 861-865.
89. Padmanabhan M, Jhaveri K, Sharma R, Basu PK, Li J. Light-induced degradation and regeneration of multicrystalline silicon Al-BSF and PERC solar cells. *Physica Status Solidi (RRL) - Rapid Res Lett*. 2016;10(12):874-881.
90. Song L, Xiu Z, Fu J, Ji Z. Controlled cooling process for efficient hydrogenation. *J Alloys Compounds*. 2017;698:892-897.
91. Payne DNR, Chan CE, Hallam BJ, et al. Rapid passivation of carrier-induced defects in p-type multi-crystalline silicon. *Solar Energy Mater Solar Cells*. 2016;158:102-106.
92. Xiang Z, Gong L, Bei W, Min Z, Bing D. Characteristics and value enhancement of cast silicon ingots. *Solar Energy Mater Solar Cells*. 2015;139:27-33.
93. Gong L, Wang F, Cai Q, You D, Dai B. Characterization of defects in mono-like silicon wafers and their effects on solar cell efficiency. *Solar Energy Mater Solar Cells*. 2014;120:289-294.
94. Sio HC, Phang SP, Fell A, et al. The electrical properties of high performance multicrystalline silicon and mono-like silicon: material limitations and cell potential. *Solar Energy Mater Solar Cells*. 2019;201:1-10, 110059.
95. Frey A, Engelhardt J, Micard G, Hahn G, Terheiden B. Investigation of fill factor losses on 20.2% efficient n-type mono-like silicon solar cells with laser contact opening. *physica status solidi (RRL) - Rapid Res Lett*. 10(2):143-147.
96. Jay F, Muñoz D, Desrues T, et al. Advanced process for n-type mono-like silicon a-Si:H/c-Si heterojunction solar cells with 21.5% efficiency. *Solar Energy Mater Solar Cells*. 2014;130:690-695.
97. Kivambe M, Kivambe MM, Haschke J, et al. Record efficiency N-type and high-efficiency P-type mono-like silicon heterojunction solar cells with high temperature gettering process. *Acs Appl Energy Mater*. 2019;2(7):4900-4906.

How to cite this article: Song L, Yu X. Defect engineering in cast mono-like silicon: A review. *Prog Photovolt Res Appl*. 2020;1-21. <https://doi.org/10.1002/pip.3364>